University of Nevada, Reno

Characterizing Spatial and Temporal Variability of Snow Water Equivalent Using Pressure Sensors

A thesis submitted in partial fulfillment of the
requirements for the degree of Master of Science in
Hydrology

by

Benjamin D. Trustman

Dr. Daniel Obrist/Thesis Co-advisor
Dr. Rina Schumer/Thesis Co-advisor

May, 2016

THE GRADUATE SCHOOL

We recommend that the thesis
prepared under our supervision by

BENJAMIN D. TRUSTMAN

Entitled

Characterizing Spatial And Temporal Variability Of Snow Water Equivalent Using Pressure Sensors

be accepted in partial fulfillment of the
requirements for the degree of

MASTER OF SCIENCE

Daniel Obrist, Ph.D., Advisor

Rina Schumer, Co-Advisor, Ph.D., Committee Member

Adrian Harpold, Ph.D., Graduate School Representative

David W. Zeh, Ph.D., Dean, Graduate School

May, 2016

Abstract

The goal of this study is to characterize spatial variability of snow water equivalent (SWE) at the meter scale. The study includes measurement of SWE with a new pressure sensor and use of meteorological sensor data to investigate physical properties within the snowpack that can affect sensor measurement. The new sensor, which can continuously measure a load equivalent to up to 5.5 meters of snow, is designed to be smaller and less expensive (< $1,500) than traditional pressure sensors (> $10,000). Manual snow cores and detailed snow pit analyses were performed to assess accuracy of the sensors and identify physical properties that may be related to sensor measurement error. SWE sensor response and accuracy were assessed between sensors and through comparison with bulk precipitation gage, manual SWE measurements, and snow pillows. SWE sensor readings compared favorably to other measurement methods, particularly in early and peak season. Spatial variability of SWE during the melt season of the two low-snow years during the study period confounded our ability to compare multiple sensor readings for validation. Spatial variability of SWE at study sites was calculated from sets of manual SWE measurements. The correlation length of 80 cm, determined using semi-variograms, highlights the small scale variability in SWE. Statistical resampling of manual measurements suggests that a minimum of ten manual measurements are needed to get within 10% of the spatial average of SWE. Although SWE can remain relatively stable during the melt period, this can be a result of increased density with decreasing snow depth, suggesting that simple inferences about SWE from depth measurements are not appropriate.

Table of Contents

List of Tables

List of Figures

1. Introduction

Melting snow is a source of fresh water that is an integral resource in many regions worldwide (Dozier 2011). Runoff from mountainous terrain provides water for municipal, commercial, recreational uses and power generation. In the Western U.S., it is estimated that 40-70% of precipitation falls as snow and that snow melt is responsible for 80% of soil moisture and stream-flow (Jepsen et al. 2012, Marks et al. 2002, Rice et al. 2011). On an annual basis, snow is the largest fresh water reservoir supporting regional water use (Mote et al. 2005). Understanding snow water equivalent (SWE), the amount of water in the snowpack, and spatial distribution patterns is essential for water management decisions in reservoir management and water allocation for irrigation in the semi-arid states located in the Western U.S. (Guan et al. 2013, Jepsen et al. 2012, Molotch et al. 2009, Rice and Bales 2010).

This study focuses on the spatial variability of snowpack (i.e., SWE, snow depth, and snow density) as this affects melt rate and the timing and volume of fresh water availability (Jost et al. 2009). SWE is defined as the height of snow (h_s) multiplied by the bulk density (ρ_s) of snow as it relates to the density of water (ρ_w):

$$SWE = h_s * \frac{\rho_s}{\rho_w} . \qquad (1)$$

Measurement of SWE by taking snow cores with a hollow tube in equal spatial increments was pioneered in the 1930's by Dr. James Church of the University of Nevada (Nevada 2012). As technology advanced, SWE was measured by automated, fluid filled

snow pillows (CDWR 1976). Both measurement methods are still in use today. As satellite imagery and multispectral measurement technology have developed, inference about snowpack SWE on larger scales has become possible (Dozier 2011). Airborne and space-borne technology requires ground based measurements in order to validate the remote sensing model estimates of SWE, but the current measurement network was not designed to support these advanced platforms (Molotch and Bales 2005, Rice and Bales 2010, Rice et al. 2011).

Large spatial and temporal variability in snowpack dynamics, including different accumulation and melt rates, pose challenges in accurately quantify snow distribution (Bormann et al. 2013, Elder et al. 1991, López-Moreno et al. 2013, Molotch et al. 2009, Watson et al. 2006a), and thus present challenges in both measurement-based and model-based estimations of water amounts. In particular, variability in snowpack density is under-studied, with snow depth measurements outnumbering snow density measurement by 30:1 (Jonas et al. 2009, López-Moreno et al. 2013, Sturm et al. 2010). Though snow depth is generally considered more variable than density, both in space and time, there is substantial variability in density even at locations only meters apart indicating that depth alone cannot be used to obtain SWE (Jonas et al. 2009, Kinar and Pomeroy 2015, López-Moreno et al. 2013). Snow density can vary as much as 30% in samples taken within one meter distance (Jonas et al. 2009, López-Moreno et al. 2013). Thus, variation in snow density should be measured rather than assumed in order to understand distribution of SWE which is both a function of depth and density (Kinar and Pomeroy 2015, NASA 2014).

SWE variability is particularly pronounced in mountainous regions, e.g., when compared to open snow fields found in the arctic and mid-west U.S. (Sturm et al. 1995). The majority of snow in the contiguous U.S. resides in western states. In these mountainous regions, topography and snow redistribution by wind play an important role in snow density which suggests that spatially-resolved measurements of both depth and density are needed to establish representative SWE values (Kinar and Pomeroy 2015, Watson et al. 2006b). Another factor contributing to density variability is snowpack evolution over time. The range of snowpack density can change over time in any location based on the influences of environmental variables such as temperature, depth, wind, and heat flux (Sturm et al. 1995). In general, snow density increases over time as snow grains within the snowpack are subject to metamorphic changes (Rasmus 2013, Sturm and Holmgren 1998). Unfortunately, with a shortage of density measurements, time-density models used to characterize snowpack evolution and SWE generally only use depth measurements (Jonas et al. 2009, Sturm and Holmgren 1998).

A warming climate will lead to changes in the timing of snowmelt, influencing the timing of streamflow which in turn can affect sustainability of water resources by altering the availability of water (Jepsen et al. 2012). Changes in temperature, wind, and precipitation regimes can have substantial effects on the snowpack evolution (Jepsen et al. 2012, Johnson and Schaefer 2002, Kumar et al. 2013, Marks et al. 2002, Molotch et al. 2009). Climate change studies indicate a decline of regional snowpack and suggest that sub-alpine ecosystems and other terrestrial landscapes in the arid west will encounter longer and more intensified periods of water stress (Bales et al. 2006, Molotch et al. 2009, Mote et al. 2005). Predictions of change from snow dominated areas to rain

dominated in the Western U.S., based on historical and predicted temperature regimes, show that snow cover will recede and peak snowpack will occur earlier (Klos et al. 2014). Large mountainous regions in undeveloped and developing countries, such as the Hindu Kush in Afghanistan, have few to no measurements of SWE yet are completely reliant on seasonal snowpack for their survival (Dozier 2011). Changes in timing of seasonal runoff can have devastating effects on crop production and the subsequent livelihood of millions of inhabitants in these regions. With roughly one-sixth of the world population living in snowmelt dominated regions and otherwise low capacity for surface water storage (Viviroli et al. 2011), potential changes in seasonal snow regimes highlight the need for increased, accurate measurements and modeling techniques.

The overall goal of this study is to characterize snowpack dynamics related to the spatial and temporal variability of SWE. The first goal is to assess the performance of a new low-cost pressure sensor to directly measure SWE both under laboratory conditions and in the field by continuous measurement of SWE and comparison to several other measurement methods of SWE, snow depth, and snow density. The new sensor is smaller (1.2 m X 1.2 m) and less expensive (< $1,500) than traditional pressure sensors (3 m by 3 m, > $10,000) and operates with battery power, allowing for multiple sensor deployment and high density measurements. The second goal is to specifically investigate physical properties within the snowpack that may induce measurement errors of the new SWE sensor, in particular by effects such as bridging and over- or under-measurement using spatial and time-series of snowpack observations and relationships to meteorological data such as precipitation, radiation, and temperatures. The final goal is to characterize spatial and temporal variability of SWE using the pressure sensors at

multiple locations as well as with manual snow cores and detailed snow pits in order to study the heterogeneity of snow packs. The study was carried out in three mountain regions of the western U.S. (Figure 1):

1) The first site was Sagehen Creek Experimental Forest (39°26’57.52” N, -120°17’07.72” W), located 32 kilometers from Lake Tahoe in the Tahoe National Forest. Sagehen has a maritime climate with a typically large, dense snowpack averaging three meters at lake level (Lake Tahoe) and up to seven meters on the peaks.

2) The second site was Snake Range in eastern Nevada (38°54’21.88”N, -114°18’31.96”W), a site with an intermountain, continental climate with typically dry, low snow density averaging one to three meters of total snowpack on the highest peaks.

3) The third site was at Mammoth Mountain Ski Resort (37°38’35.21” N, -119°01’44.88” W); located on the eastern side of the southern Sierra Nevada Mountains, a site that exhibits the characteristics of both maritime and continental climate regimes. Mammoth is known for deep snowpack characteristic of the Sierra Nevada Mountains but can exhibit a drier and less dense snowpack compared to the western side of the Sierra Nevada.

Figure 1. SWE pressure sensor locations 2013-2015

2. Goals and Questions

Goal 1: Assess the viability and accuracy of a new load cell pressure sensor design in measuring SWE by comparing pressure sensor measurements with bulk precipitation gages, snow pillow and manual snow cores for direct SWE measurements.

Question 1: Is the pressure sensor accurately measuring SWE during both accumulation and melt in the different climate regions?

Goal 2: Investigate the timing and cause of pressure sensor errors using a suite of meteorological sensors and manual snowpack analysis.

Question 2: If the pressure sensor is not working correctly, what are the reasons for potential measurement errors?

Goal 3: Characterize spatial variability of SWE using pressure sensors and manual snow measurements.

Question 3: What is the degree of SWE spatial variability at the meter to tens of meters scale and how does variability in snow depth and snow density compare?

Question 4: How does SWE variability differ across the three mountain regions used in this study, and is it driven by variability in density, depth or both?

3. Background Information

3.1 Measurement of Snow Water Equivalent

There are two commonly used techniques to directly measure SWE in the field: manual snow courses and automated snow pillows. A snow course consists of several manual snow core measurements taken in selected locations 20-100 meters apart. Cores are taken with a tube that has a sharpened end to cut through snow layers and weighed. This method produces both depth and density measurements that can be used to calculate SWE. Manual snow cores sampling was pioneered by Dr. James Church at the University of Nevada, Reno in the 1930's. Church's Mt. Rose Federal Sampler (or also called Standard Federal) and variations of it are still widely used in snow course measurements. A snow course produces a snapshot of SWE distribution in time. Snow courses are usually performed once or twice a year at locations chosen for maximum snowpack (Rice et al. 2011). These snow courses are employed preferentially over snow pit analysis to characterize the spatial distribution of the snowpack for two reasons: first, the snow-tube is far less destructive to the snowpack than a snow pit; second, a snow pit analysis consists of digging a pit with squared walls to the bare ground surface and taking a sample of specific volume at graduated increments on the wall. Though this technique is the most accurate (Dixon and Boon 2012), it is by far the most time consuming of all the available methods. In the early 1960's, a new tool was developed to measure the

mass of a snowpack through the use of a fluid filled snow pillow. This is an automated system that provides continuous SWE data throughout the snow season. By the late 1970's, the U.S. Soil Conservation Service began to implement a network of automated SNOpack TELemetry (SNOTEL) sites using snow pillows to provide data from high snow accumulation regions (Doesken and Schaefer 1987). Currently the Natural Resources Conservation Service (NRCS) has 666 active SNOTEL stations in the Western U.S. (Figure 2). In addition, California has 98 active snow sensors run by several agencies including the California Department of Water Resources, U.S. Bureau of Reclamation, U.S. Army Corps of Engineers, and several water utility districts.

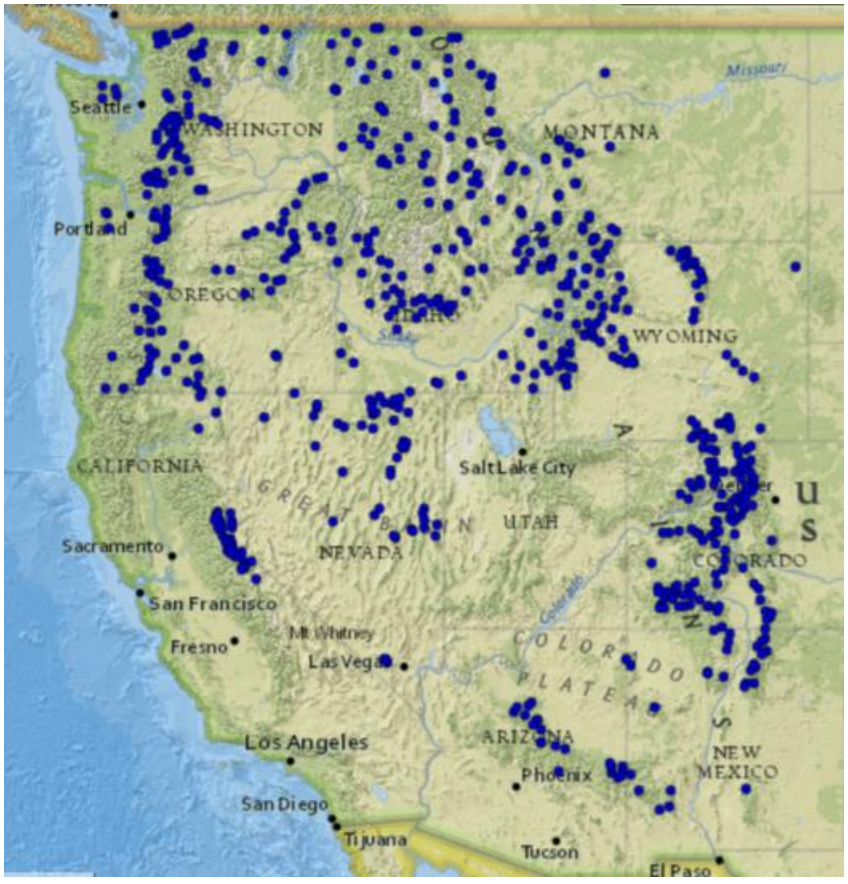

Figure 2. Active NRCS SNOTEL stations from the Rocky Mountains to the Western of the U.S. (www.wcc.nrcs.usda.gov)

SNOTEL sites are either outfitted with rubber pillows or galvanized metal pillows filled with fluid. A pressure transducer located in a standpipe measures the fluctuation of fluid driven by weight distributed on the pillow (CDWR 1976). Original pilot studies found that pillows measuring less than 3.04 m in diameter or having less than 4.6 m^2 surface areas did not consistently register snowpack under all conditions found in the Sierra Nevada mountains (CDWR 1976). The large size of the snow pillow sensor and its accompanying station requirements creates limitations on the placement of SNOTEL sites based on topography and, in many cases, permitting. In recent years, sensors that measure snowpack mass, like a snow pillow, have been developed using load cell technology. An electronic load cell is a transducer that converts a mechanical force into an electronic signal, which can be calibrated to monitor SWE and eliminate the need for a fluid filled pillow. A multi-year field study was conducted using an array of load cell sensor designs to assess viability of use for SWE measurement and source of sensor measurement errors (Johnson et al. 2014, Johnson and Schaefer 2002). Through design modification and comparison with manual measurements, a design was created that was determined to work as effectively or better than existing snow pillow sensors.

There are several other new methods that have been developed to measure SWE in recent years. Campbell Scientific developed a SWE sensor that measures terrestrial gamma radiation and its changes in attenuation through a snowpack (Campbell Scientific, Logan, UT USA). Ground penetrating radar and dielectric tape are also used. All of these emerging technologies have limitations based on cost (gamma radiation), depth of snowpack (ground penetrating radar), and location and installation constraints. None of

these products, however, have been employed in large scale snow observation projects such as SNOTEL.

Measuring snow water equivalent and snow density accurately is inherently difficult. The Standard Federal sampler has shown between 6 to 11% overestimation when used properly, compared to snow pit measurements (Dixon and Boon 2012). Errors in proper core sampling can be caused by numerous factors. First, a snow core should measure ≥80% of the snow depth, but this can be difficult due to collapsing of the snowpack layers during insertion of the corer as well as snow that could be lost through the slotted sides that are shaved off from twisting action as the tube is inserted to the snow. A soil plug acquired with the core sample (which is removed before weighing) ensures a full sample was taken, but sometimes does not exist due to the ground conditions (e.g., when rocks are present). Without a soil plug there can be loss of snow from the sampler as the core is removed from the snowpack.

The accuracy and precision of snow pillows depends on site characteristics, equipment and installation techniques. Many inherent issues, such as fluid leakage or damage caused by wildlife, can be mitigated through design (Cox et al. 1978). However, measurement inaccuracies are caused by physical snowpack dynamics such as ice layer formation and differential melting during freeze/thaw cycles (Johnson 2004a, Johnson et al. 2007, Johnson et al. 2014, Johnson and Marks 2004, Johnson and Schaefer 2002). For example, SWE over- or under-measurement is often attributed to edge effects or bridging. Snow bridging occurs when some or all of the mass of a snow load is transferred to the surrounding snow, typically due to snow melt or vapor gradient flow to the snow above

the sensor (Johnson et al. 2007, Johnson et al. 2014; Figure 3). Bridging most commonly occurs during freeze/thaw periods, when the snow is undergoing a diurnal melt cycle. The sensor has different thermal properties than the surrounding soil which causes a change in water vapor gradients resulting in snow melt at the sensor surface. Sub-freezing nighttime temperatures refreeze the water and in turn can create a void space above the sensor. Physical properties of snow during rapid settlement can also cause edge effects. Errors attributed to differential snow settlement occur when stress concentrations along the perimeter of the sensor increase due to rapid settling following a heavy snowfall event as well as when snowmelt rates at the sensor differ from snowmelt rates at the ground surface (Johnson et al. 2007, Johnson et al. 2014). Error magnitude is a function of the freeboard (distance of the sensor above ground surface; Figure 3) of the sensor and viscosity of the snow.

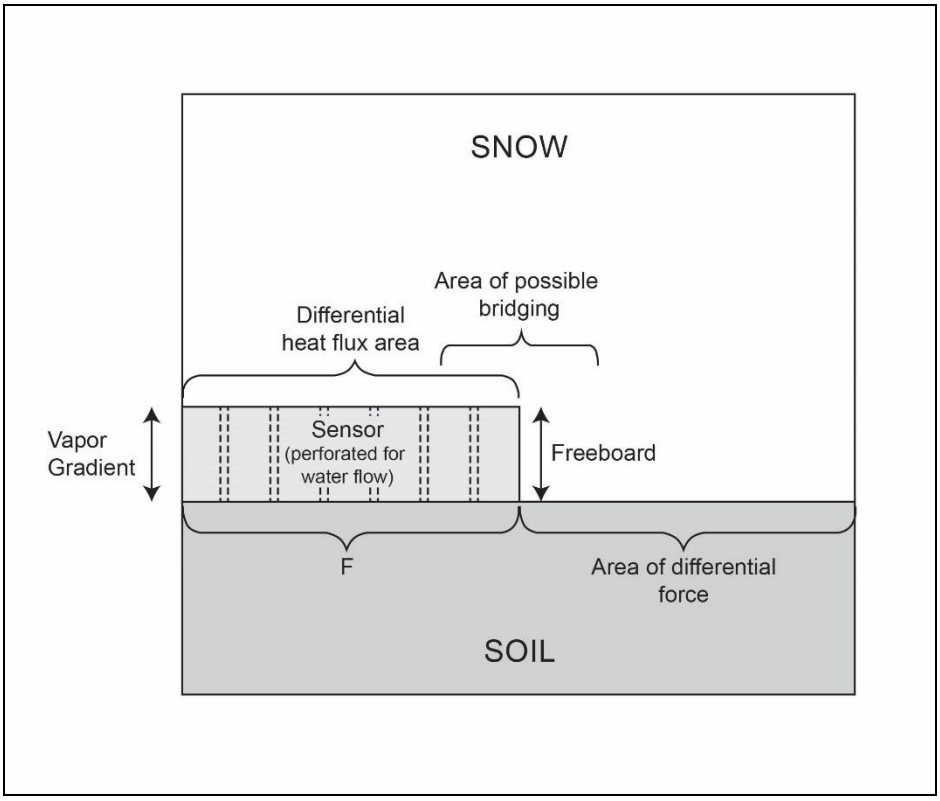

Figure 3. Example of sensor error potential for the electronic load cell ground based pressure sensor.

SWE over-measurement errors in load cell pressure sensors occur when there is lower heat flux through the sensor than the surrounding soil. SWE under- measurement errors occur when the heat flux through the sensor is greater than surrounding soil (Johnson and Schaefer 2002). These errors can be prevented by reducing the height of the sensor from the ground surface (freeboard), and by using perforated sensor material to allow water flow and heat exchange through the sensor to the soil surface. When errors occur at sites with independent snow depth measurements, corrected SWE values (SWE') are calculated using a reference snow density (ρ_{ref}) based on the average snow density and depth (h_s) at the start of the sensor error (Johnson et al. 2007). Correction equations

are used until SWE sensor measurement and error corrected measurements intersect (Johnson and Marks 2004).

Initial snow density is given by,

$$SWE' = \frac{\rho_{ref}}{\rho_w} h_s \qquad (2)$$

where

$$\rho_{ref} = \frac{h_s}{SWE} \rho_w \qquad (3)$$

and ρ_{ref} is reference snow cover density at the time prior to the error.

A key limitation of SWE measurement is the high cost of equipment or manpower. Beginning with manual core samples, which give a measurement of depth, density and SWE at one point in time, it has been estimated that one site visit for several samples would take 1 hour of time for two people (Watson et al. 2006a). The cost of manual snow coring can increase rapidly when adding drive time and several sites visits over long distances. Core sampling also presents limitations in mountainous terrain due to accessibility and avalanche danger. Use of snow machines and helicopters can further drive up costs. Manual samples produce one SWE value for one moment in time, and as snowpack changes over the season, collection of multiple measurements is recommended for accuracy of water estimation. Snow pit sampling is far more labor intensive and intrusive to sampling sites rendering them impractical for multiple sampling schemes. The snow pillow was designed to take continuous measurements throughout the snow season, but their large size and high cost limits deployment location. A snow pillow

bladder alone can cost more than $4,000, and a full SNOTEL site kit including the snow pillow, bulk precipitation standpipe, and transducers costs approximately $8,000 (Rickly Hydrological Company, Columbus, OH USA). These costs do not include the metal net (over $2,000) that is placed on top to deter prevent bears from damaging bladders. The actual cost of installation, including instrumentation of weather station, telemetry and permitting for a SNOTEL station can cost over $35,000 (personal communication, Michael Strobel Ph.D., Director of USDA Natural Resource and Conservation Service, National Water and Climate Center).

3.2 Spatial Variability of SWE, Snow Depth, and Snow Density

Snowpack distribution at the watershed scale is influenced by timing of accumulation, wind redistribution, temperature, elevation, and aspect of a landscape (Bormann et al. 2013, Jonas et al. 2009, López-Moreno et al. 2013, Meromy et al. 2013a, Molotch and Bales 2005, Sturm et al. 2010, Watson et al. 2006a). At the plot scale, accumulation and wind redistribution can be affected by micro-topography, preferential deposition, interception in forested areas, and local advection creating unpredictable snowpack variability (Clark et al. 2011, Jost et al. 2007). Causes of spatial variability in a snowpack can be divided into two categories: fixed factors, which are predictable parameters such as elevation, vegetation, slope and aspect, and unpredictable factors such as micro-topography or small scale changes in ground surface, fallen logs, tree wells and small scale wind effects (Watson et al. 2006a). Snowpack also undergoes metamorphosis almost immediately after snowfall, leading to redistribution and modification of the snowpack density (Dixon and Boon 2012, Pomeroy 1995, Watson et

al. 2006a). Climate and snowpack age have strong effects on the variability of snow density as well as depth of the snowpack. Spatial variability in snowpack density decreases over the season as the dominant drivers of density transition from temperature and wind during accumulation to snow metamorphosis or ripening during melt (Jonas et al. 2009, López-Moreno et al. 2013). Temporal and spatial variability complicates up-scaling of SWE from point measurements to grid values for large scale SWE model estimations (Clark et al. 2011, Liston 2004, López-Moreno et al. 2013, Sturm et al. 2010, Winkler et al. 2005).

Depth measurements outnumber SWE measurements 30 to 1 and the dynamic range of snow depth across spatial gradients can be up to 4 times greater than that of density (Sturm et al. 2010). In spite of a smaller range, snow density ranges by 5-32% in samples taken within 1-10 m. (Jonas et al. 2009, López-Moreno et al. 2013). In mountainous terrain, small topographical changes can have large effects on density. Thus, in order to make an accurate SWE measurement, both snow depth and density must be measured. The disparity in depth to density measurements is a function of the effort required for each. Manual snow depth measurements can be taken quickly and efficiently with visual snow stakes or a snow probe. Newer digital snow probes have memory and GPS for automatic logging in the field (e.g. Avatech, Park City, UT, USA). Automated snow depth sensors are widely used in remote weather stations and are relatively inexpensive ($100-700) compared to pressure sensors used to measure SWE (see introduction). Airborne LiDAR (Light Detection and Ranging) that can take large numbers (n>5,000) of accurate snow height measurements above ground to 1 meter resolution has become a popular technique to estimate snow depth. LiDAR is used to

derive snow depths by measuring areas when snow is not present and then re-measuring the same area at specific times throughout the snow season. Though LiDAR can produce accurate depth measurements over larger areas, density measurements are still required to estimate SWE. Studies using airborne LiDAR have shown that ground based depth measurements are typically placed in areas of higher than average snow depth (Grünewald and Lehning 2015). LiDAR cost far exceeds that of manual measurements based on expenses for flight time which include crew, fuel, and airplane. In order to get a depth measurement a minimum of two flights need to be performed.

Advances in remote sensing have broadened the option for large scale measurement of SWE and assessment of spatial variability across large scales. Several parameters of snow can be detected using spectral reflectance. Estimates for albedo and grain size can be obtained through these signatures (Dozier 2011, Guan et al. 2013, Molotch and Bales 2005, Rice et al. 2011). Multispectral signatures can also be translated to snow covered area in complex mountainous terrain (Dozier 1989, Jicheng et al. 2008). Passive microwave attenuation though the snowpack is another measurement that can be made from remote sensing. This technique can be translated into SWE and depth but has limitations in deeper snowpack (Dietz et al. 2012). Furthermore, all remote sensing based models rely on some ground measurements for calibration and validation. Many measurements are needed to characterize the spatial variability of depth, density and in turn SWE and the costs associated with large scale ground measurement are currently prohibitive (Rice and Bales 2010, Watson et al. 2006a)

3.3 Sensor Development

For this project, a new pressure sensor to measure SWE was designed using a load cell. A Loadstar ™ RAP3 single point load cell (Loadstar Sensors, Freemont, CA USA; Figure 4) with a 500 lb. (226.8 kg) capacity and 250% total overload capacity is used under a 45.72 cm, diameter 6.35 mm aluminum sensor. The circular weigh sensor is centered in a 1.2 m x 1.2 m, 6.35 mm aluminum sensor. The outer square is an inert area designed to accept the edge effects that cause bridging. The weigh sensor and outer square are both perforated with 6.35 mm holes roughly every twelve to fifteen cm (Figure 5). Perforations allow water to flow through the sensor and saturate the soil surface underneath to limit the heat differential between saturated soil adjacent to the sensor and the sensor itself. The difference in heat flux occurring at sensor surface and the adjacent soil can lead to bridging. The weigh sensor sits on two aluminum sensors attached to the square outer area and sit roughly seven cm below the surface. The whole inert area is framed by 2.54 cm x 3.8 cm aluminum square tubing. The sensor, pictured below, is installed flush to the soil surface and anchored by metal rebar that is placed through holes in the excess square tubing at all four corners (Figure 5).

Figure 4. Loadstar RAP3 single point resistive load cell.

Figure 5. SWE sensor at the sub-alpine west site in the Snake Range, NV.

The RAP-3 is a strain gauge load cell. A strain gauge load cell consists of four resistors configured to create a Wheatstone Bridge (an electrical circuit measuring two legs of a bridge circuit, unbalanced and balanced). The resistors are attached to a stainless steel block that bends as force is applied to a single point. The resulting strain generates an electrical signal measured in millivolts per volt of input (mV/V). This signal is sent to a data logger (CR800 and CR1000; Campbell Scientific, Logan, UT, USA).

3.4 Sensor Calibration and Verification

In order to measure SWE, a conversion coefficient between the electric signal and the mass applied to the sensor must be generated. First, in the laboratory, weight calibrations were performed for each sensor using buckets with varying amounts of water and specified weights to generate a conversion coefficient between the electric signal and the mass applied to the sensor. This coefficient was created to calculate mass from

millivolts. The first set of sensors was calibrated using water in five gallon buckets (Figure 6). An initial test was performed to assess if there was a difference in the weigh sensor measurement when the sensor was clamped to the workbench as opposed to when it was secured to the sensor frame. This test showed minimal difference in measurements between the workbench and the sensor frame, so all subsequent calibration measurements were carried out with the sensor weigh sensor secured to the workbench for simplicity. An empty bucket was weighed for a tare weight. Five liters of water was added for each measurement until the bucket was full. Another tare weight was taken after adding another bucket on top. This process was continued until a total of thirty liters (30 kg) of fluid was added. This calibration process was performed on each of the first six weigh sensors. All recorded values were entered into a spreadsheet and tares removed to associate water to millivolts. Centimeters of SWE was calculated by equating liters of water to cubic centimeters then dividing the volume by the area of the weigh sensor.

The results of regression analysis of the millivolt response of the load cells and the weight added provided in this chapter were all statistically significant ($P<0.05$-data not shown). The slopes for the sensor calibration varied from 75.09 to 78.93, and all showed high linearity ($r^2 \geq 0.999$.) For the 2013-2014 winter season, an average slope of 76.57 from the six calibration points was used as a multiplier in the data logger program for SWE measurement readings. The data logger was programed to take ten minute measurements of maximum SWE, minimum SWE, average SWE, as well as the raw millivolt readings from the sensor and create an hourly average measurement. The raw

millivolts are recorded in case any post collection data processing needed to be performed.

After the 2013-2014 winter season, a set of five 2 kg calibration weights were purchased for field calibrations to be performed after the sensors were snow free. In order to verify the performance and linearity of the SWE cells in real conditions, we also performed calibrations directly with installed sensors in the field. Post-season calibrations were done on two sensors, SWE 1 and SWE 4 (referring to SWE 1 and SWE 2 at Subalpine West). Here, results showed a change in slope of +4.84 cm for SWE 1 and +2.39 cm for SWE 4 compared to previous laboratory calibrations, or a 6 % and 3 % change, respectively. The results were outside of the manufacturers calibration of repeatability which was <0.02 %, but were within the manufacturers calibration for linearity of <0.02 % with $r^2 \geq 0.999$. Therefore, installed load cells were subject to some differences in signal response compared to the load cells in the laboratory. These differences may be attributed to several things, including changes in environmental conditions (e.g. temperature), cable length affecting voltage (e.g. as the cable length increases the excitation voltage can degrade based on signal loss, thus lowering the amount of signal the sensor is receiving and then returning based on the principles of the circuitry), and diurnal power fluctuation (e.g. increase in power distribution with increased solar input).

A second set of six sensors, built in 2014, were calibrated in the laboratory using the 2 kg weights (Figure 7). The slopes for this set of sensor calibrations varied between 75.06 and 79.92, and all calibrations were highly linear ($r^2=1.0$). The data loggers were

programed using the individual slope coefficients for each sensor for the 2014-2015 winter to increase measurement accuracy. Previously deployed sensors were also assigned new coefficients for the winter 2014-2015 season based on field calibrations prior to the winter.

Figure 6. Calibration of weigh sensors using water and five gallon buckets.

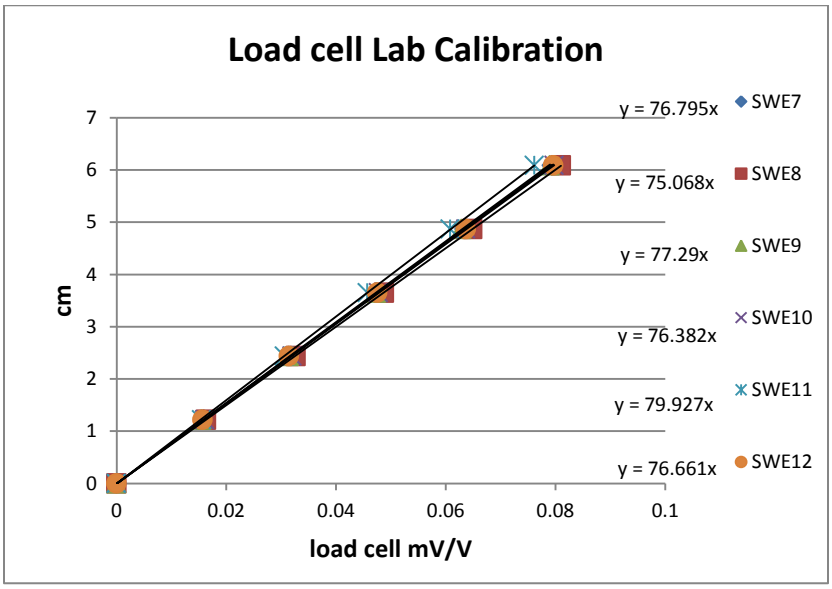

Figure 7. Conversion coefficients for SWE sensors built for 2014-2015 winter using the 2 kg weights for the laboratory calibrations.

4. Study Sites

4.1 Study Sites 2013-2014

Five SWE sensors were deployed at sites with a series of existing meteorological and environmental instrumentation. Three sensors were placed in the Snake Range, Nevada which is located 97 kilometers southeast of the city of Ely, NV (see Figure 1). This mountain range is home to the northern transect of the Nevada Climate-ecohydrology Assessment Network (NevCAN http://nevcan.dri.edu) and the Great Basin National Park. This network consists of climate monitoring stations that include measurement temperature, total precipitation and several other parameters (see Table 1), over elevations ranging from 1,560 meters to 3,355 meters. The two highest elevation sites, Subalpine West (two sensors elev. 3,355 m) and Subalpine East (one sensor elev.

3,070 m), are snow-dominated peaks that receive between one and four meters of snow annually. A total of five SWE sensors were placed in the field as summarized in Table 1. The sensors at the Subalpine West site were strategically placed in a shaded, wind protected area and in a sun exposed area (Figures 8 and 9). The sensor at the Subalpine East site is within fifty meters of, and has similar exposure to, the Wheeler Peak SNOTEL site (station 1,147, National Resource and Conservation Service) that measures SWE with a snow pillow. An additional SWE sensor was located at the Sagehen Creek Field Research Station, located in the Sagehen Creek Experimental Forest watershed 18 kilometers north of Truckee, CA. The Sagehen Research Station has a number of meteorological data sensors, including four snow pillows that measure SWE. The load cell SWE sensor was placed within five meters of the snow pillow at Sagehen's Tower 1 site (elev. 1,957 m). This sensor was placed as close as possible to the snow pillow to compare measurements in a similar exposure. A fifth SWE sensor was installed at the Alpine Meadows Ski Resort (elev. 2,121 m) located between Truckee, CA and Tahoe City, CA. The resort is situated on Ward and Scott Peaks in the Lake Tahoe Basin, in the Ward Creek watershed. The sensor was placed at the base of the resort adjacent to the Roundhouse chairlift. The resort collects meteorological data, including temperature, bulk precipitation, snow depth, and event based SWE that can be used for comparison to the sensor.

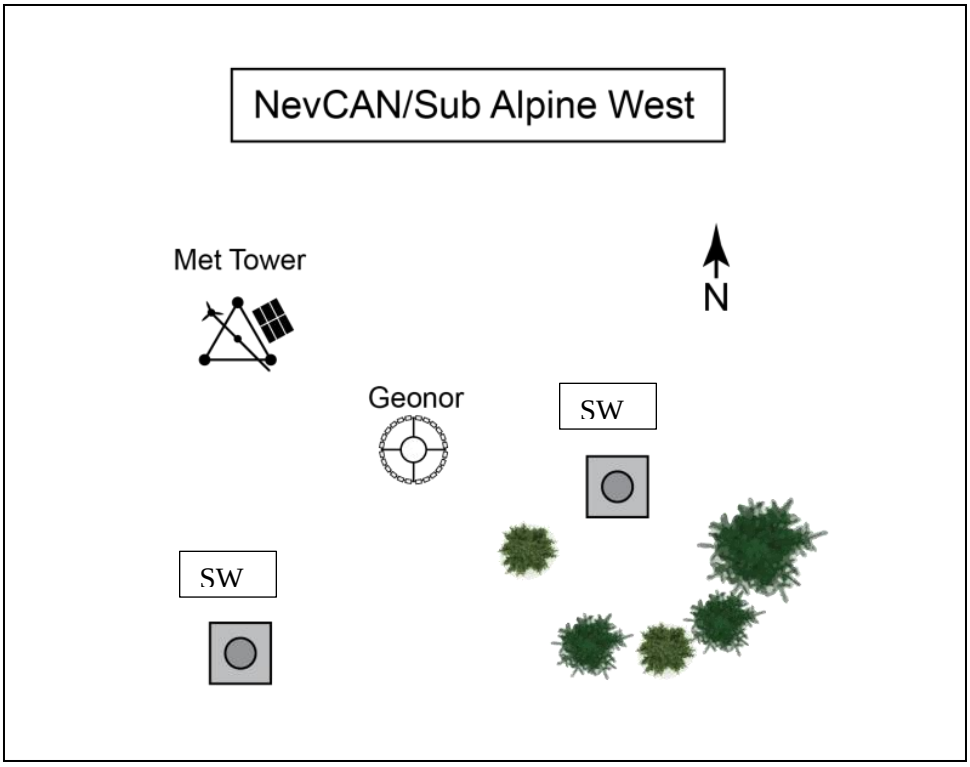

Figure 8. Schematic of sensor deployment at Subalpine West in the Snake Range, NV 2013-2014.

Figure 9. Sensor installation at Subalpine West 10/26/2013.

4.2 Study Sites 2014-2015

Two additional SWE sensors were deployed at the NevCAN subalpine west site in the Snake Range, Nevada (elev. 3,355 m). These sensors were placed next to the existing sensors to create replicate measurements (Figure 10, 11 and 12). The Sagehen Tower 1 sensor was moved to the Tower 3 site (elev. 2,118 m) and three additional SWE sensors were installed at the site. These sensors were placed between 5 and 30 meters of the snow pillow at the Tower 3 site. The sensors are arranged in a wooded area from under canopy to open area. This arrangement is designed to assess the variability of the SWE as it relates to forested settings. Three sensors were installed at the CRREL UCSB Eastern Sierra Snow Study Site (CUES http://snow.ucsb.edu/) located on Mammoth Mountain, CA (elev. 2,940 m). The sensors are located in an area with minor topographical variation adjacent to the instrument tower. One sensor was placed next to the ultrasonic depth sensor (Ultrasonic Snow Depth Sensor, Judd Communications, Salt Lake City, UT, USA), one out in the open, and one next to the snow pillow. The arrangement of these sensors allowed a snow course (manual cores) to be performed between sensors. This installation is in a location that is expected to have relatively high homogeneity in the snow distribution.

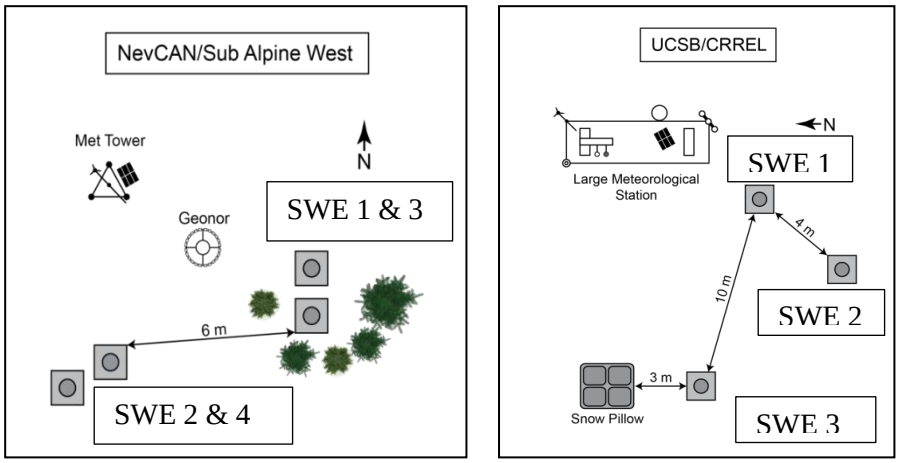

Figure 10. 2014-2015 sensor deployment at Mt Washington, NV and Mammoth Mountain, CA

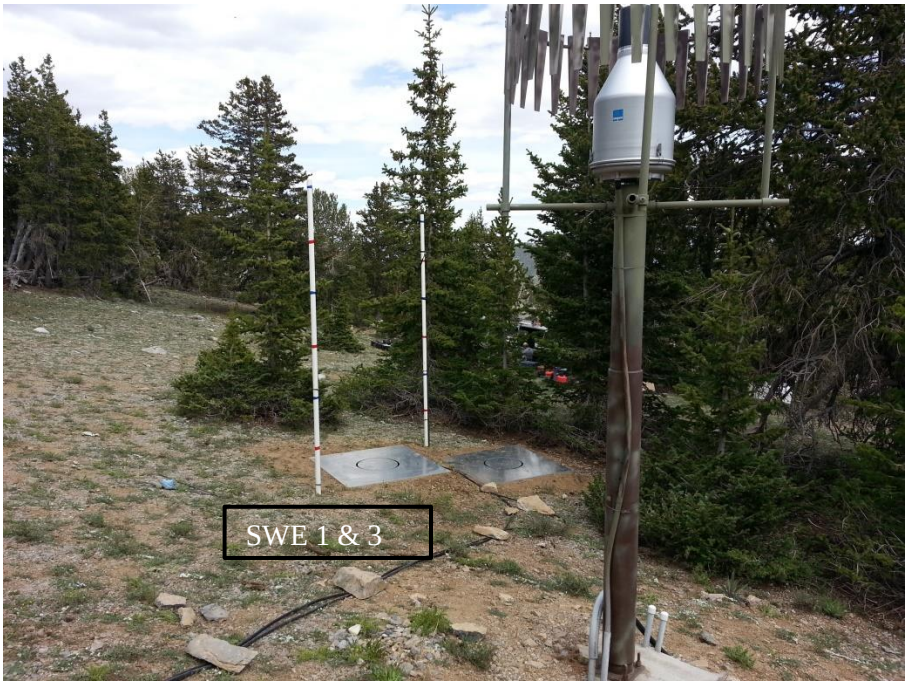

Figure 11. Subalpine West protected zone installation June 2014.

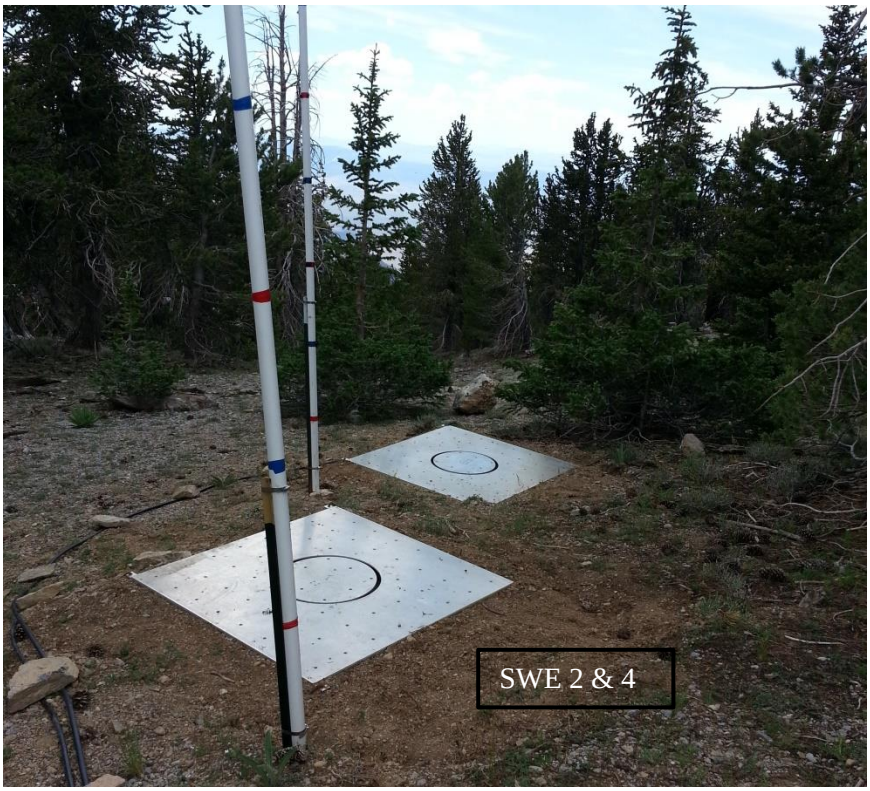

Figure 12. Subalpine West exposed zone installation June 2014.

Table 1. Locations of load cell SWE sensors and additional meteorological measurements available at each site.

Site Name	Location	Elevation (m)	Number of SWE sensors	Other measurements available
Alpine Meadows	Alpine Meadows Ski Resort, Lake Tahoe, CA	2121	1	Air temperature, bulk precipitation, snow depth (manual and ultrasonic), precipitation event based manual SWE
Subalpine East	Great Basin National Park, Snake Range, NV	3070	1	Air temperature, bulk precipitation, snow depth, soil moisture, solar radiation, SNOTEL SWE (50 meters away)
Subalpine West	Mt. Washington, Snake Range, NV	3355	4	Air temperature, bulk precipitation, snow depth, soil moisture, solar radiation
Sagehen	Sagehen Creek Experimental Forest Watershed, CA	2118	4	Air temperature, snow depth, soil moisture, solar radiation, SWE (snow pillow)
Mammoth	Mammoth Mountain , CA	2940	3	Air temperature, snow depth, soil moisture, solar radiation, soil water flux, SWE (snow pillow)

5. Validation of SWE Sensors in the Field and Laboratory

5.1 Methods

5.1.1 Sensor Validation and Testing

Analysis of the load cell sensor response to accumulation and ablation of snow was performed by comparing the sensor data to other instrument readings. The replicate sensors located at Subalpine West were compared to each other and to visual depth measurements as well as to bulk precipitation data. The sensor at NevCAN Subalpine East climate station was compared to the Wheeler Peak SNOTEL (NRCS station #1147) snow pillow and to onsite snow depth data. The sensors located at the CUES snow observatory in Mammoth, CA were compared to the snow pillow located onsite as well as to ultrasonic depth measurements. Manual snow cores taken adjacent to sensors were used to assess the variability of SWE. A snow pit was dug at each site visit to measure SWE by taking samples every 10 cm using a 1000 cm^3 Kelly wedge cutter (Model: RIP 1 Cutter; Snowmetrics, Fort Collins, CO, USA). Two sets of Kelly cutter samples were taken from each pit. Hence, validation of the sensors was determined by the response to laboratory and field tests using water (in buckets or snowpack) and weights. Due to high spatial variability of SWE at small scales (<1 m), a number of samples were taken at small distances to provide confidence intervals of SWE to test if the SWE sensor measurements fell inside these intervals.

5.1.2 Snowpack Physical Measurements to Assess Sensor Errors

Pressure sensor errors can either be caused by physical properties of the snowpack or by electronic malfunction. During the season, real time data was monitored to assess onset of errors. Troubleshooting was performed in the field after electronic malfunction of a load cell was discovered from erroneous data. Manual snow pits were analyzed to create profiles of snow layers during each site visit to understand the layering of snowpack. This process consisted of digging a 1.5 m^2 pit to the ground surface. Measurements of height, density and grain size of layers were noted for each identifiable layer using the a standardized protocol (Snow, Weather and Avalanches: Observational Guidelines for Avalanche Programs in the United States [SWAG]; American Avalanche Association, 2010) Hourly camera images of the sensors from the NevCAN sites were also used to profile layering events and identify snow coverage of sensors. Other meteorological data were examined to estimate snowpack dynamics including, temperature (all sites), precipitation (all sites), solar radiation (NevCAN, Mammoth), soil temperature and moisture (NevCAN, Mammoth), soil surface water flux (Subalpine west), sensor temperature using thermistors (Mammoth), and hourly camera images (NevCAN, Mammoth). Using some of this data, a timeline of snowpack layering and dynamics was constructed and verified by the pit analysis.

5.2 Results and Discussion: SWE Sensor Validation and Testing

This study was performed during two winter seasons of a four-year drought. The April 1, 2014 snowpack in the Sierra Nevada was 18% of the long-term average

snowpack (CDWR 2014) and showed a record low of about 5% of long-term average in 2015 (CDWR 2015). The warm temperatures and lack of precipitation produced very little to no snowpack at the Sagehen site; there was very little sustained snowpack at the Tower 1 and Tower 3 locations, thus there were no usable data from the Sagehen sites over the 2013-2014 and 2014-2015 winter seasons. The sensor placed at Alpine Meadows in the winter of 2013-2014 responded to accumulation and ablation, but meteorological data used for comparison were unreliable. The results in this section therefore focus on laboratory tests of the SWE sensors, the field tests with weight in the absence of snowpack, and the SWE sensor field performance at the two eastern Nevada sites and the Mammoth Mountain site.

5.2.1 Laboratory Testing of SWE Sensors

In addition to SWE sensor calibrations, further weight testing was performed in the Desert Research Institute Hydrology Technical Laboratory to validate the stability of a sensor under an estimated maximum load. In order to calculate a realistic maximum load, a peak SWE value of 184 cm (307 kg) was chosen from water year 2011 at the Central Sierra Snow Laboratory (39°20’ N;-120°22’W, Norden, CA, Donner Summit: elev. 2089 m, established in 1943). This location is known for its large maritime snowpack and the 2011 water year SWE was estimated at ≈165% of the 30-year average SWE from 1981 through 2010 for the Sierra Nevada Mountain Range (Zito 2011). Fifteen 20.4 kg weights were added to multiple sensors in increments of 40.8 kg over several days to assess maximum load capacity and sensor drift. A calibration was also performed using five 20.4 kg sensors was performed on SWE 1 and SWE 3. Calibration

results remained highly linear (SWE 1: r^2=0.9999; SWE 3: r^2=0.9998). The slopes of these calibrations were not the same as those of previous calibrations because the tests were performed using 5V excitation, whereas the earlier calibrations used 2.5V excitation. Tests were conducted over several days to evaluate sensor drift (Figure 13).

The sensor initially failed to continually record data at 224.4 kg; this failure was because the flex of the measurement sensor exceeded the distance created by a spacer between the sensor and the load cell. The measurement sensor came into contact with the opposite side of the load cell, thus negating the strain on the gage (Figure 14). A second spacer was added to the sensor so it could accept the maximum load of 306 kg (Figure 15). Long time tests were used to test for measurement drift. The first test was performed with 40.8 kg of weight over 1,440 hours. The sensor measurement varied from 1.68 mV to 1.70 mV, resulting in an overall drift of ±0.003 cm. A second test was performed with a maximum load of 306 kg for roughly 63 hours. The sensor measurement varied from 12.22 mV to 12.25 mV, resulting in an overall drift of ±0.5 cm. The sensor drift, although changing with increased load, is comparatively small (0.01% at 40.8 kg and 0.16% at 306 kg) and does not affect accurate measurement of SWE. Furthermore, the drift in measurement fluctuated over time, representative of sensor noise rather than systematic error (Figure 16). - The maximum SWE of 184 cm from the Sierra Snow Laboratory in 2011 is equivalent to roughly seven meters of snow (calculated using the mean normalized density from manual measurements taken in the spring of 2015 for this study). The Sierra Nevada snow depth is at the high end of the range with its maritime climate, with as much as 5 to 7 m at higher elevations in average and above-

average years, whereas depth in the Rockies, Alps and Pyrenees typically ranges between 2.5 to 4 m (Jonas et al. 2009, López-Moreno et al. 2013, Molotch and Bales 2005). The results of the laboratory tests show that the pressure sensor design can accept the snow load from any of these representative snow-dominated locations. Furthermore, the stability of the sensor under continual load suggests that the pressure sensor would be able to accurately measure the SWE over the prolonged winter season with minimum drift in signal.

.

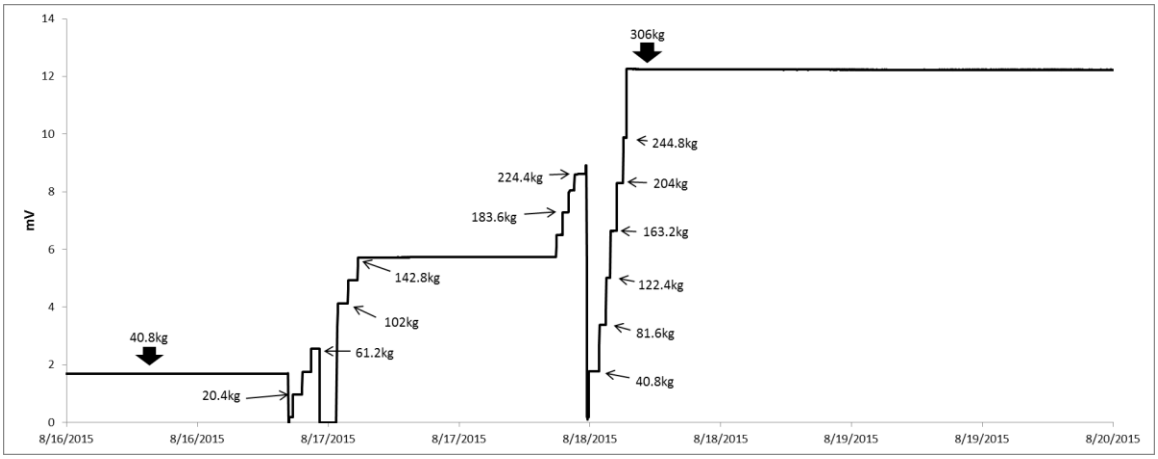

Figure 13. Laboratory tests show a time series of load cell sensor response to increased weight up to a maximum load of 306 kg.

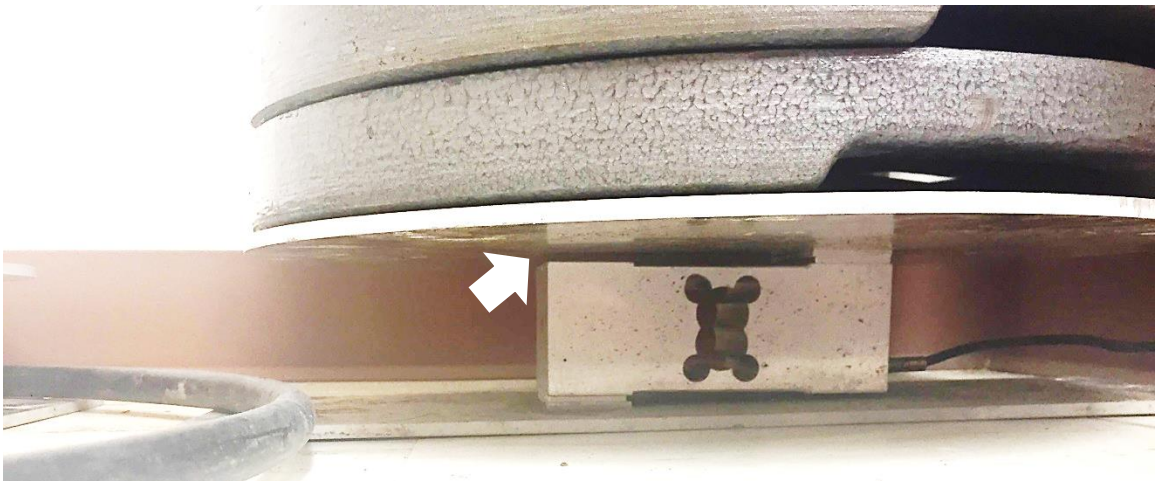

Figure 14. Load cell with two spacers. The arrow points to the connection point when the load cell stopped measuring due to overload of the single spacer at 224.4 kg.

Figure 15. Laboratory test with a load of 306 kg, equivalent to 184 cm of SWE.

Figure 16. SWE sensor measurement fluctuates over the time period, due to electrical circuitry. The total change in measurement was equal to± 0.003 cm over this time period.

5.2.2 Field Tests of SWE Sensors

Field calibration tests were performed at the Sagehen and Sub-alpine West study sites in the fall of 2014. Each sensor was tested using five 2 kg weights. Results for the four sensors at the Sub-alpine West sites had slopes varying from 77.79 to 83.77 and the four sensor field calibrations at Sagehen results had slopes varying between 78.01 and 81.14. Hence, all results of the field tests showed a high linearity of sensor response in the field ($r^2 \geq 0.9998$ at Sub-alpine West; $r^2 = 1.0$ at Sagehen), with some differences in slope between sensors occurring possibly as a result of field installation. These changes from laboratory testing reinforce the need for field calibration of the new SWE sensors in order to ensure maximum measurement accuracy.

5.2.2.1 Field Comparison of SWE Sensors to Other Measurements at Sub-alpine West, Mt. Washington, Snake Range, NV

2013-2014 Winter Season Sensor Comparison

Two SWE sensors from the 2013-2014 winter season were compared to a bulk precipitation gage (Figure 17). A shaded area sensor (SWE1) showed a strong response with increased mass, reflecting accumulation of snow, and the temporal patterns of mass increase coincided well with precipitation as recorded by a bulk precipitation gage. A full sun exposure sensor (SWE 2) showed less response to new precipitation, possibly due to frozen layers in the snowpack discovered during snow coring. It is important to note that the bulk precipitation gage only measures increases in precipitation and not decreases due to melt or sublimation, and therefore for this comparison only increases in mass were examined. Increases in SWE recorded by the pressure sensor were compared with increases observed in the bulk precipitation gage (Figures 18 and 19). The results from the SWE 1 sensor measurements were linearly correlated with those of the precipitation gage (r^2= 0.9967; slope of 1.39). It can be interpreted from a slope with a value of greater than 1.00 indicates that the increase in bulk precipitation does not translate to the same direct change in the pressure sensor measurement, as shown in Figure 17 where SWE 1 measured 40% more SWE than the precipitation gauge. The bulk precipitation gage has a small opening (15.9 cm) and is situated 2.5 meters above ground with an Alter shield to reduce wind effects, and therefore only measures the direct input of precipitation from the atmosphere. The pressure sensor, on the other hand, is located on the ground and can have inputs from both atmosphere and wind redistribution. More importantly, bulk precipitation gages have continually shown bias towards under-catch of precipitation caused by wind, even those that are present with wind protection (Savina et al. 2012, Yang et al. 2000). Furthermore, while precipitation gages give

inherent errors typically attributed to under-catch, ground-based sensors give inherent errors from redistribution and wind transport as well as edge effects (Johnson 2004a, Johnson and Marks 2004). However, the relationship in SWE accumulation measured by the two sensors suggests that both sensors showed precipitation response at the same time, but differences may have been from errors such as those described above.in either sensor or spatial variability. A site visit was performed in the spring of 2014 to the Sub-alpine West site in the Snake Range, NV, in order to conduct manual SWE measurements around the two pressure sensors and to physically characterize the snowpack. Sets of 8-10 SWE measurements were taken using a Mt. Rose Federal sampler on March 15, 2014, at 1 m increments directly adjacent (<1 m) to each sensor. Manual SWE measurements taken in 1 meter increments adjacent to shaded pressure sensor SWE 1 ranged from 15-28 cm. The mean measured SWE was 23 cm, with a coefficient of variation of 17%. Samples collected adjacent to sun-exposed pressure sensor SWE 2 ranged from 17-27 cm. The mean SWE was 22 cm, with a coefficient of variation of 17% (Figure 20). The pressure sensor measurements were not in the range of the manual measurements, but were within ± 3 standard deviations of the manual measurements, reflecting high variability of SWE within 1-10 m (López-Moreno et al. 2013). The mean of the two sensors was within 8% of the mean of the manual measurements, suggesting that multiple measurements of SWE by replicate sensors may reduce uncertainties induced by spatial variability.

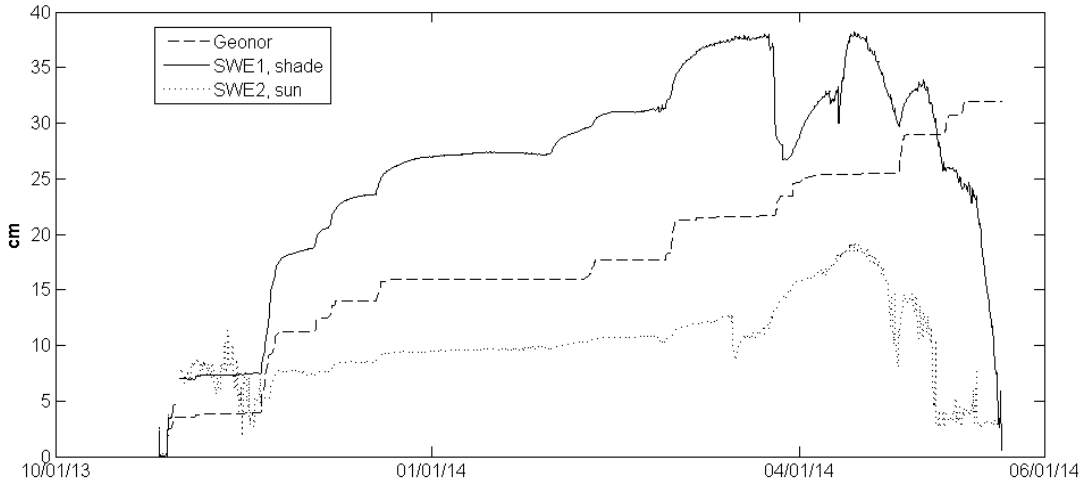

Figure 17. 2013-2014 Sub-alpine West SWE sensors and bulk precipitation (Geonor).

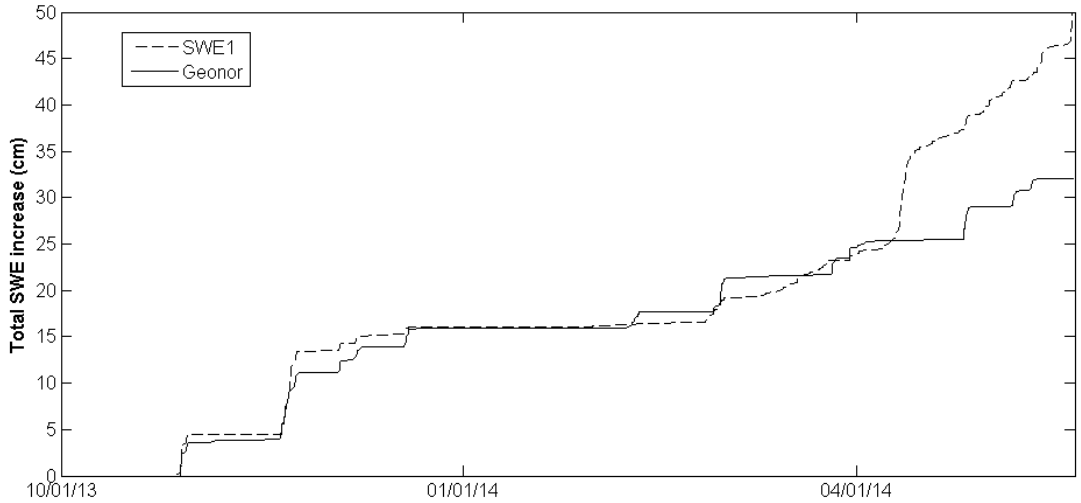

Figure 18. Cumulative increase of SWE1 compared to the bulk precipitation gage. Later season response and increase differences can be due to sensor errors caused by snow bridging that resolve when the snowpack becomes isothermal (uniform temperature of 0° C) and begins to melt, thus redistributing the mass onto the sensor.

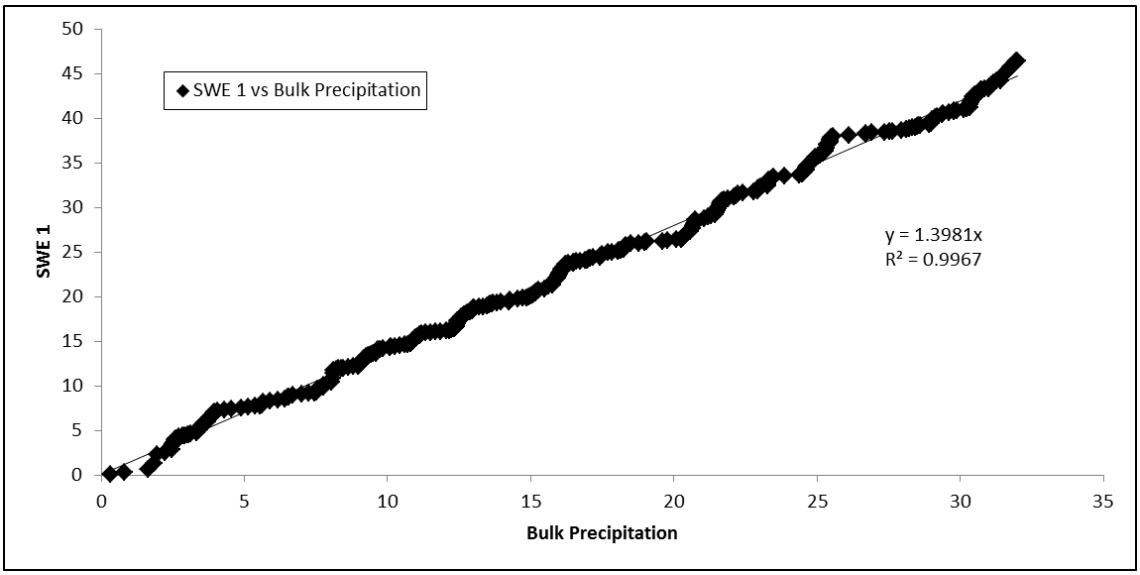

Figure 19. SWE sensor increase compared to bulk precipitation gage increase. The r^2 shows excellent linearity, but the slope shows a difference in measurement between the instruments of between 35-40%.

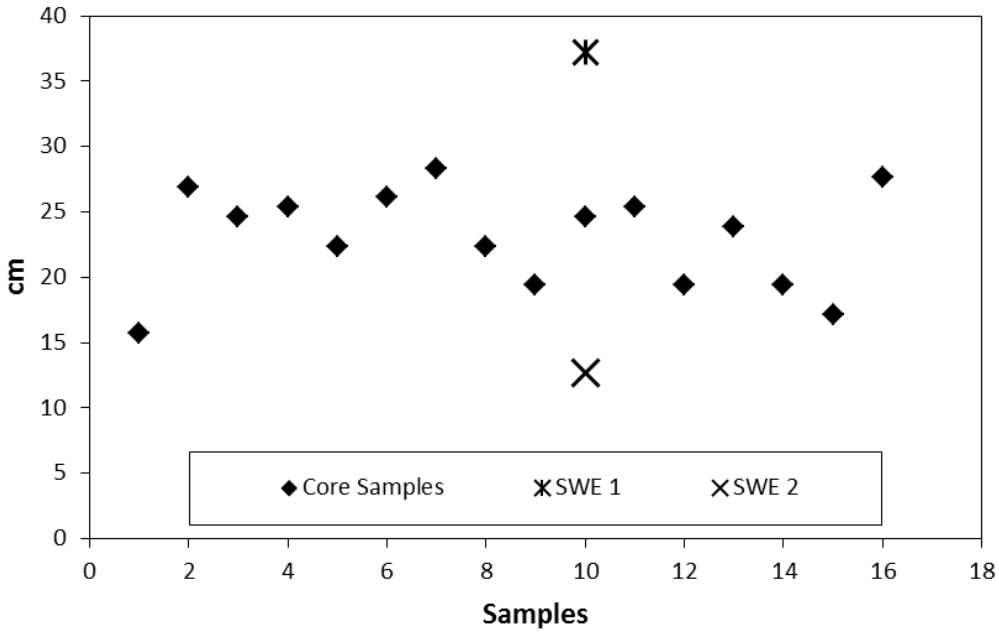

Figure 20. Results of 16 manual SWE measurements. These were between 15 and 28 cm of SWE with a mean of 23 and a standard deviation of 3.82. The SWE sensors measured 13 cm (sun) and 38 cm (shade).

2014-2015 Winter Season Sensor Comparison

Two additional SWE sensors were installed next to the existing sensors at Sub-alpine West for replicate measurements during the 2014-2015 winter season. Measurements from the two replicate SWE sensors were strongly correlated (unless otherwise noted; see below). Small, early season storms don typically create a continuous snowpack. Analysis of the change in SWE (Δ SWE) from -November and December showed better agreement than the data from the individual sensors from the previous winter. ΔSWE between the two shaded load cells (SWE 1 compared to SWE 3) was strongly linear with a coefficient of determination, r^2= 0.89 and slope=0.83. The sun-exposed pair of load sensors, SWE 2 and SWE 4, exhibited a lower coefficient of determination (r^2= 0.68) and a much lower slope=0.49 (Figure 21). Late fall precipitation events typically result in ephemeral snowpack, which supports the results of the comparison since the shade protected sensors (SWE 1 and SWE 3) can retain the snowpack longer than the sun exposed sensor pair (SWE 2 and SWE 4). During accumulation to peak periods from December to April, the sensors had better agreement between the paired measurements: ΔSWE of the shaded sensors (SWE 1 and SWE 3) were strongly linear (r^2= 0.96) with a slope near unity (1.005), similar to the excellent correlation of the sun-exposed pair (SWE 2 and SWE 4; r^2= 0.97; slope of 0.9983; Figure 22). The strong agreement between both sets of sensor pairs during accumulation is consistent with the result from the 2014 season comparison to snowfall amounts as assessed with bulk precipitation measurements. These results clearly show that the sensors are responding to the direct input of new snow on existing snowpack. Finally, during late-season melt phase from April until melt-out when the snowpack was

extremely variable, ΔSWE results show that the sun-exposed sensors had better agreement, with a slope of 1.05 and an r^2=0.75, while the shaded sensors were not significantly correlated (Figure 23). The large difference during this time period is attributed to the shaded sensors having different melt rates; SWE 3 was located slightly downslope and closer to trees, and had less exposure to solar radiation. Early-season and melt-period phase results are consistent with previous studies that have shown a high variability in SWE caused both by variability in depth and density during these times (Jonas et al. 2009, López-Moreno et al. 2013, Pomeroy 1995, Rasmus 2013). Specifically, ephemeral snowpack characteristic of early season precipitation events is more pronounced in the sun (Pomeroy 1995). This may be reflected by stronger correlation between the shaded sensor pair than the sun-exposed sensor pair. The paired sensors had excellent agreement during the accumulation to peak of the snowpack, which is a good indication of the accuracy of sensor response to input and continuous load.

Two separate field site visits were made in the winter and spring of 2015 to acquire manual SWE measurements and physical snowpack characterization surrounding the four load sensors. The first set of 16 snow cores was taken on February 21, 2015, in 1 m increments directly adjacent (<1 m) to each sensor. The second set of 60 snow cores was taken on March 21, 2015, as a transect starting 16 m downslope and continuing 30 m upslope of the sensor area, covering a total area of 73 meters. Snow cores were taken at intervals of 0.2 m (adjacent to the sensors), 1 m, 3 m, and 5 m, respectively. On each visit, snow pits were installed within 5 m of the sensors. SWE from snow cores taken in February ranged from 13 to 22 cm adjacent to the shaded sensors, with a coefficient of

variation of 18%. SWE of the snow cores from sun-exposed locations (or adjacent to the sun-exposed load cells) ranged from 14 to 26 cm, with a higher coefficient of variation of 24%. Sixty snow cores were taken during the March site visit, and SWE values ranged from 10 to 28 cm, with a coefficient of variation of 22% (Figure 24). Therefore, SWE at this site in the vicinity of the load cell sensors showed a high degree of variability, which needs to be taken into account when assessing sensor accuracy (Johnson and Schaefer 2002). Whisker plots of sensor readings (Figure 25) demonstrate the uncertainty in each time series measurement. Sensor response for the co-located sensors fell within one standard deviation of the manual snow core measurements until melt phase (Figure 25).

A high degree of variability during melt phase also was confirmed by daily photos of snow stakes placed next to each sensor, and these photos were analyzed to construct snow depth profiles (Figures 26 and 27). The angle of the camera did not allow visual confirmation of both snow stakes 1 (shade) and 2 (sun) below 30 cm, so snow depths lower than 30 cm were assessed only from snow stakes 3 (shade) and 4 (sun). The snow stakes were marked at 10 cm intervals, and 5 cm estimates of snow depth were made by consulting the photos for each day. Although SWE is a function of both depth and density, the depth comparisons can serve as another independent validation of the response of the co-located sensors. SWE 1 had much lower snow depth and melted out before SWE 3 (Figure 26). The comparison of depth measurements to the sun-exposed sensors shows sensor response to smaller late-season inputs after an initial melt-out had occurred as well as the larger late-season storm. The magnitude of the SWE measurements during the late-season storm is consistent with previous studies of seasonal

density patterns of snow, with late-season snow having a much higher density (Jepsen et al. 2012, Jonas et al. 2009, López-Moreno et al. 2013, Pomeroy 1995, Rasmus 2013) .

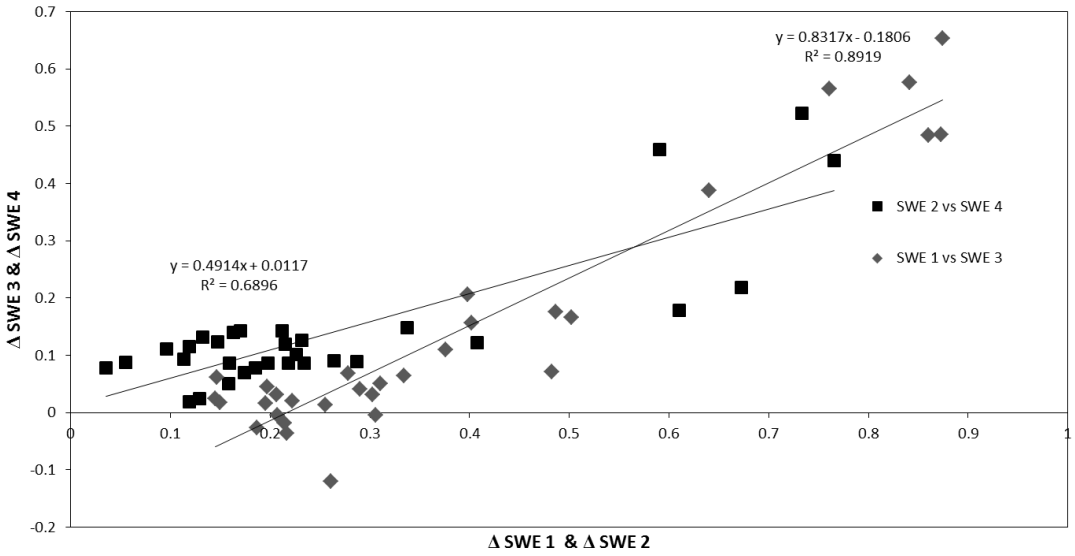

Figure 21. Early-season comparison of SWE sensor pairs located at the NevCAN Sub-alpine West site. The shade-protected sensors SWE 1 and SWE 3 had better correlation, with an r^2=0.89, compared to the sun-exposed pair of SWE 2 and SWE 4 that had an r^2=0.69.

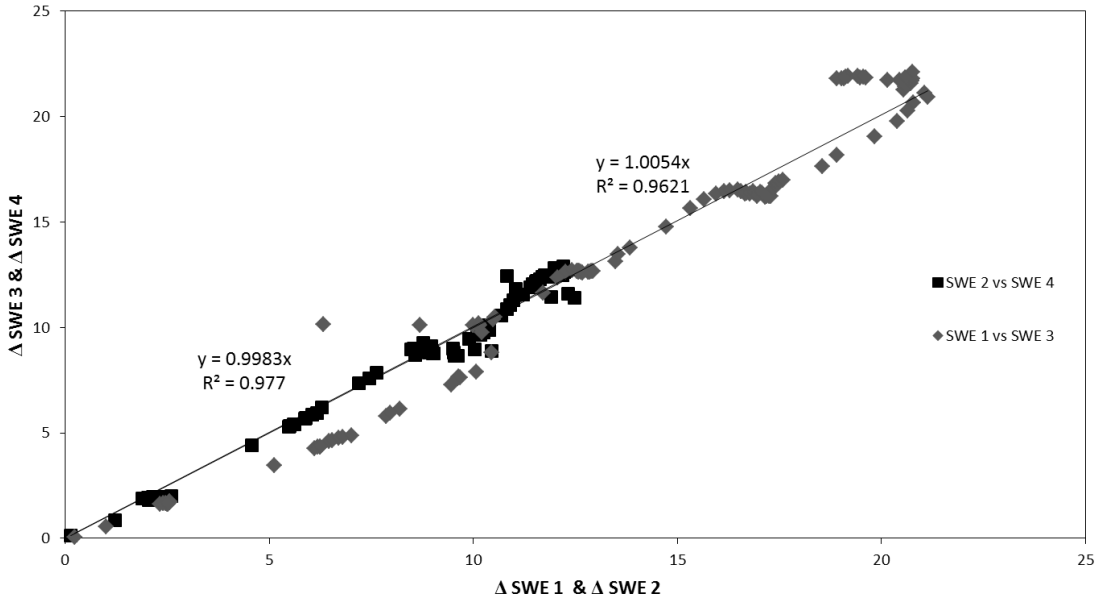

Figure 22. Comparison of the changes in SWE during accumulation periods until peak snowpack height for sensors 1 versus 3, and 2 versus 4, to validate response and measurement of SWE sensors.

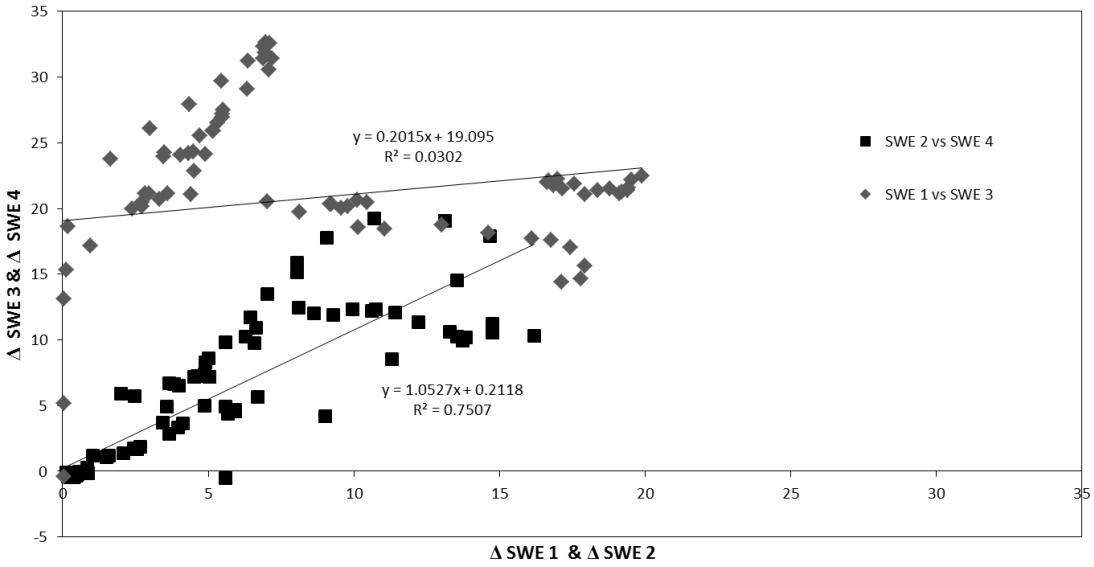

Figure 23. Comparison of changes in SWE during the melt phase show that direct exposure to solar radiation by sensors SWE 2 and 4 results in better agreement than the shade-protected sensors SWE 1 and 3.

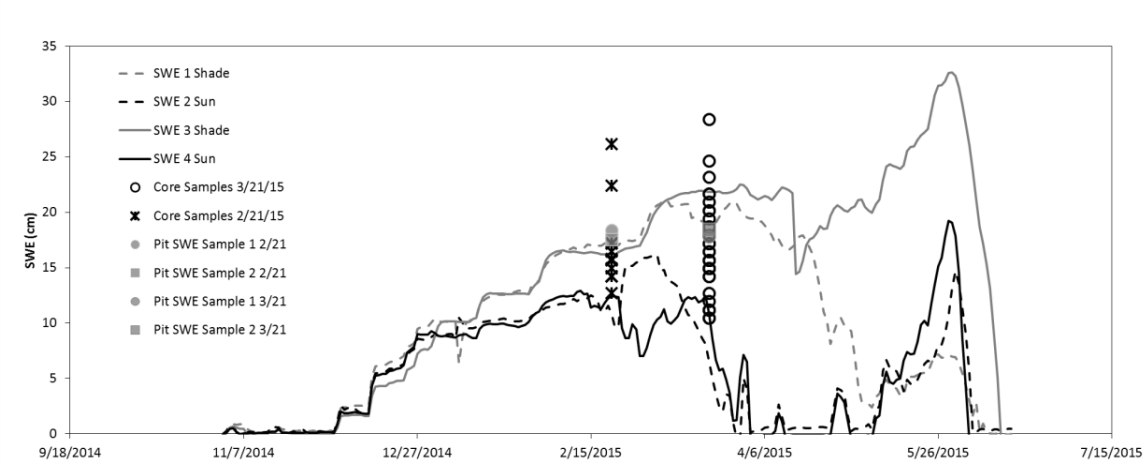

Figure 24. 2014-2015 winter season time series from NevCAN Sub-alpine West site with replicate SWE sensors.

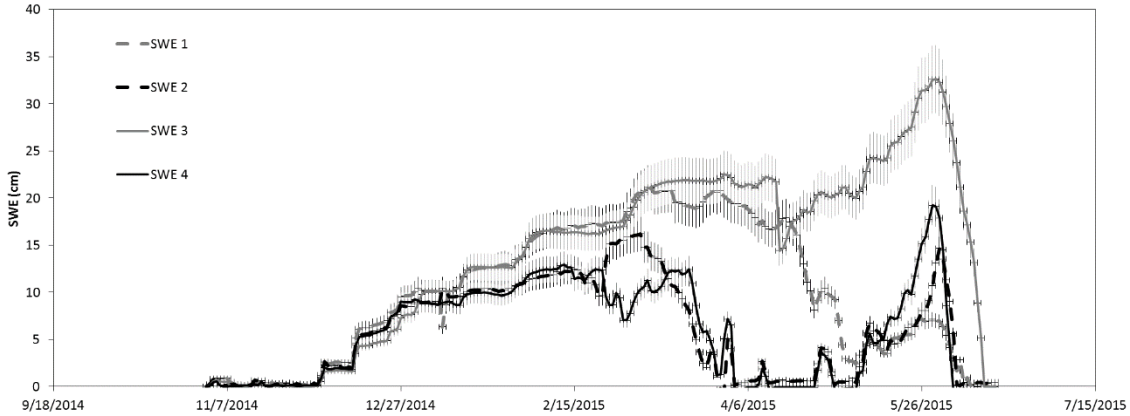

Figure 25. SWE sensor data with whiskers representing the 22% coefficient of variation from the snow core samples taken from 0.2-5 meters apart.

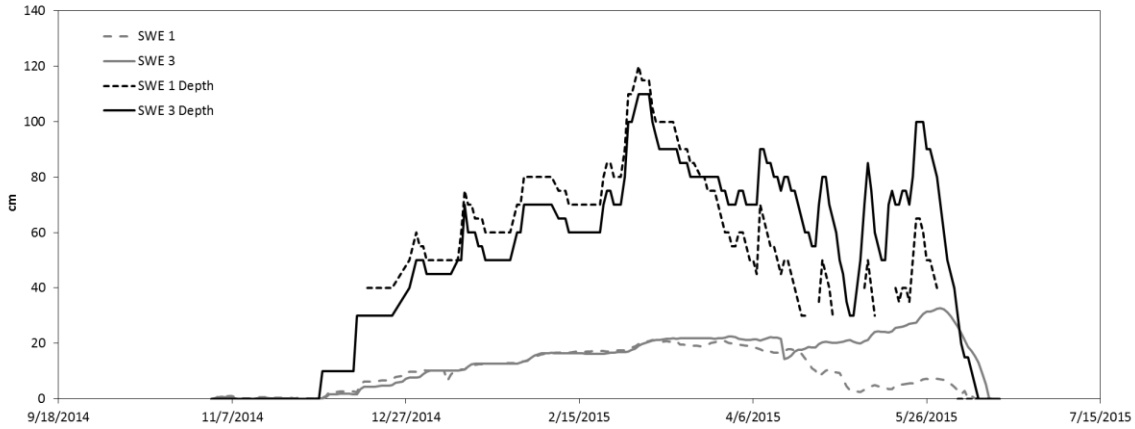

Figure 26. Shaded sensors 1 and 3 compared to the visual depth estimates.

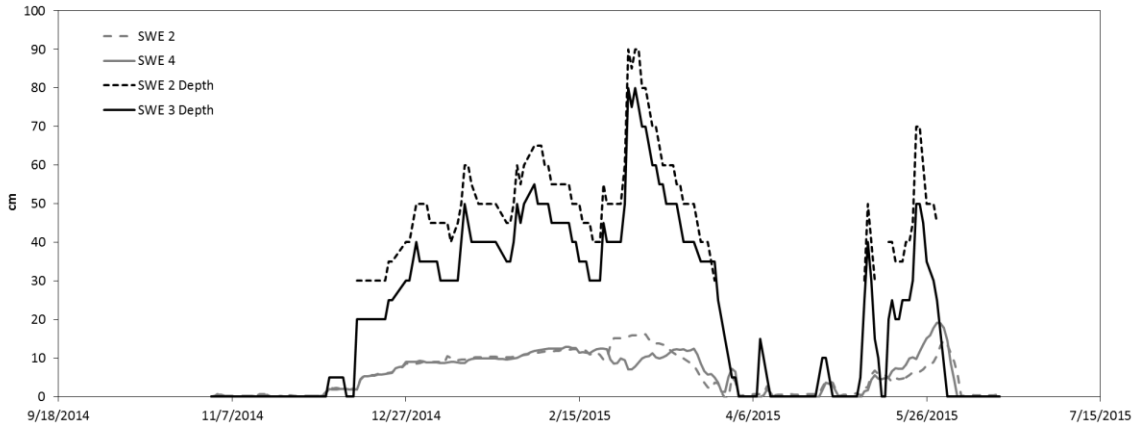

Figure 27. Sensors SWE 2 and 4 located in the sun-exposed area compared to visual depth estimates.

5.2.2.2 Field Comparison of SWE Sensors at Sub-alpine East to Wheeler Peak SNOTEL Station, Great Basin National Park, Snake Range, NV

A first load cell at this location was defective in the 2013-2014 winter and no data was available for that season. The defective load cell was replaced by the manufacturer the following spring. The 2014-2015 winter season data of one load cell was compared to the Wheeler Peak SNOTEL (NRCS station #1147) snow pillow located 50 m from the load cell sensor (Figure 28). The time series for the daily SWE values for the SNOTEL and load cell sensor agreed well when there was a snowpack, but showed differences in the early-season intermittent snowpack and the late-season melt. Early-season snowpack is intermittent, with fluctuating temperatures, whereas late-season melt is different due to density of snowpack and sun exposure. Linear regression of the SWE sensors compared to the SNOTEL snow pillow for early-season intermittent snowpack and late-season melt resulted in slopes of 0.47 and 0.34 and coefficients of determinations of 0.50 and 0.39, respectively (Figures 29 and 30). The accumulation period for the sensors was

determined by the start of continual snowpack. Comparing the SWE sensor data to those from the SNOTEL pillow for the period of record from the start of accumulation to the peak SWE showed good agreement, with the linear regression resulting in a slope of 0.98 and an r^2=0.98 (Figure 31).

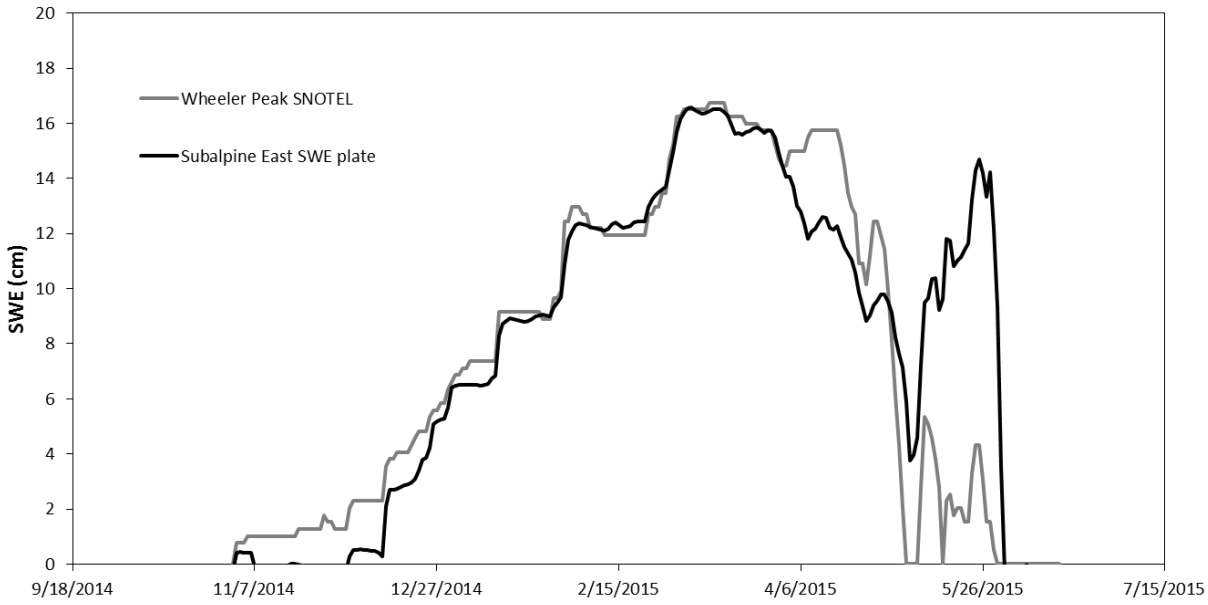

Figure 28. Comparison of data from Sub-alpine East SWE sensor and Wheeler Peak SNOTEL station snow pillow.

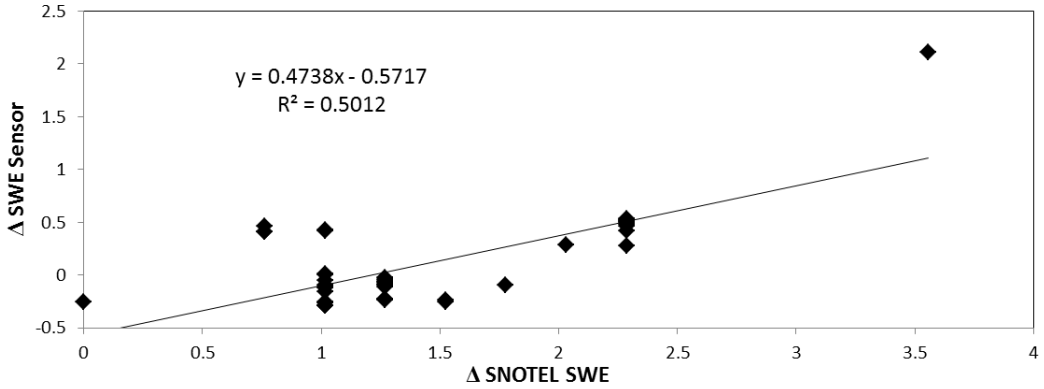

Figure 29. Early-season comparison of the ΔSWE of the SNOTEL snow pillow and the load cell SWE sensor at Sub-alpine East. The sensors did show some similar response to early-season storms but the distance between the sensors can account for the differences in actual measured SWE, as early season snowpack can be highly variable.

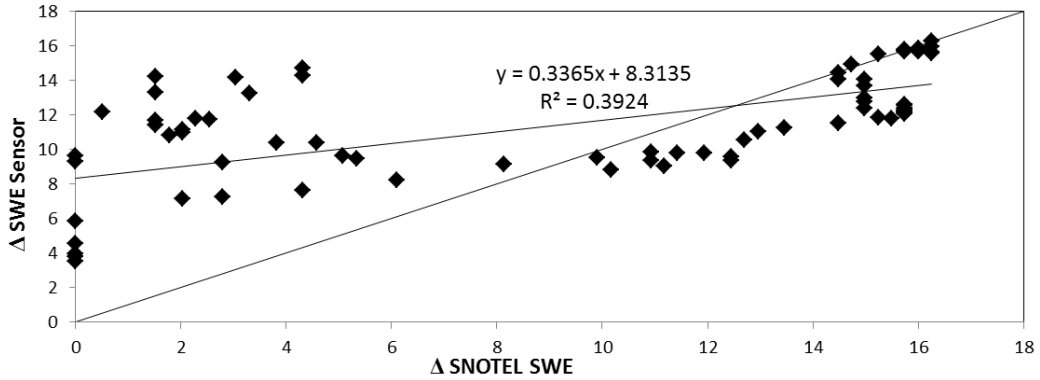

Figure 30. Melt phase ΔSWE showed high variability between the sensors.

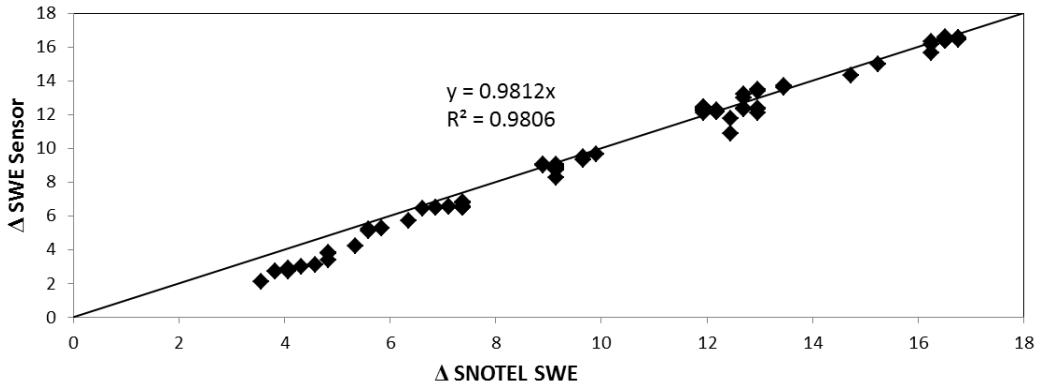

Figure 31. ΔSWE during snowpack accumulation to peak for the SNOTEL pillow and the Sub-alpine East SWE sensor.

5.2.2.3 Load Cell Performance and Comparison to the Snow Pillow at the CRREL UCSB Eastern Sierra Snow Study Site (CUES), Mammoth Mountain, CA

At Mammoth Mountain, SWE sensor data were compared to the snow pillow data (Figure 32). A load cell (SWE 3) was installed less than 3 m away from the snow pillow. A second load cell, SWE 2, was placed approximately 6 m away from the snow pillow in a flat, open area, and a third load cell (SWE 1) was located roughly 10 m away from the snow pillow next to a wind mast depth sensor. Though expected to have a more homogeneous snowpack than other study sites, the three sensors and the snow pillow documented spatial variability in SWE. This can be a product of the micro-topography and the wind redistribution of the snow within the study area (Rice and Bales 2010, Sturm and Holmgren 1998, Sturm et al. 2010). Linear regression of early season ΔSWE for each sensor reflected the spatial variability characteristic of intermittent snowpack. Regression of SWE 1 against the snow pillow showed a slope of 0.52 and an r^2=0.52. Regression analysis of SWE 2 against the snow pillow showed a slope of 0.98 and an r^2=0.46. Lastly, regression analysis of SWE 3 to the snow pillow, located just adjacent to it, showed a slope of 1.22 and an r^2=0.56 (Figure 33). The ΔSWE during accumulation to peak showed better agreement among the sensors and the snow pillow, with regression slope of 0.70 and an r^2=0.93 for SWE1, a slope of 0.34 and an r^2=0.97 for SWE 2, and a slope of 0.80 with an r^2=0.95 for SWE 3 (Figure 34). All but one linear fits was statistically significant. SWE1 likely experienced an electrical malfunction in the sensor from water in the wiring junction box (discovered after the season). Evidence of this can be seen in Figure 32 when SWE 1 began to have different response behavior to input

starting in December 2014, which ended with sensor failure in March 2015. ΔSWE of sensors 2 and 3 were compared to the snow pillow during melt (Figure 31). Regression results showed good agreement between the sensors and the snow pillow with a slope of 0.80 for SWE 2 and a slope of 1.09 for SWE 3; both having an r^2= 0.88. The melt-phase results at the CUES site are similar to the sun-exposed sensors at the NevCAN Sub-alpine West site, as the two SWE sensors and the snow pillow all receive equal amounts of solar radiation. This result is supported by studies that show that increased solar radiation due to sun angle is a driver of snow melt in open exposed areas (Guan et al. 2013, Jepsen et al. 2012, Molotch et al. 2009). Though there was general agreement between SWE 2 and the snow pillow, there was a high p-value of 0.29. This is likely due to bridging from a thick ice lens that was discovered during manual snow core sampling in March 2015. This ice lens likely caused an underestimation of SWE starting in late December 2014 until mid-March 2015, at which time the snowpack became isothermal and the sensor showed a steep increase in SWE of 10 cm, although the snow depth was declining (Figure 32). This type of error is common in ground-based pressure sensors as well as the recovery of actual SWE measurement when the snowpack becomes isothermal (Johnson 2004a, Johnson and Marks 2004, Johnson and Schaefer 2002, Johnson 2002)

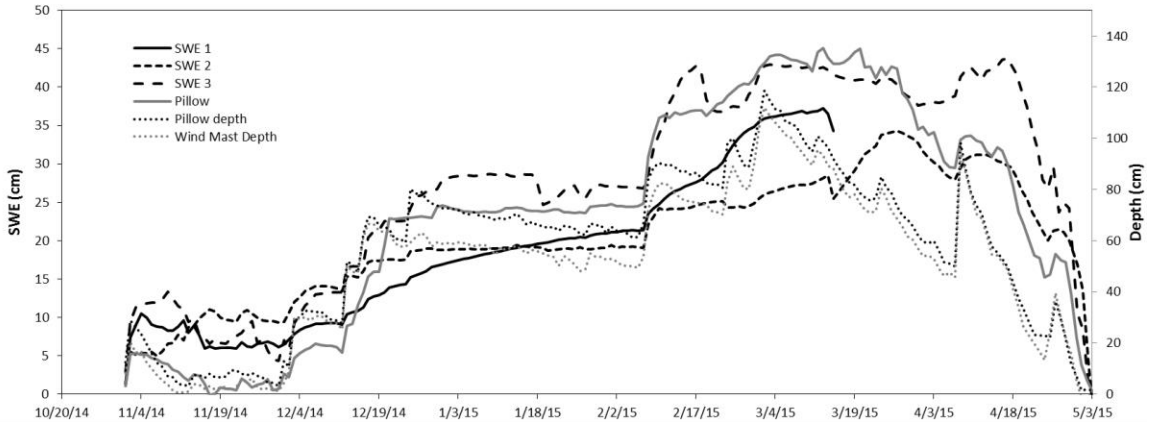

Figure 32. Comparison of three SWE sensors to the snow pillow during the 2014-2015 winter season.

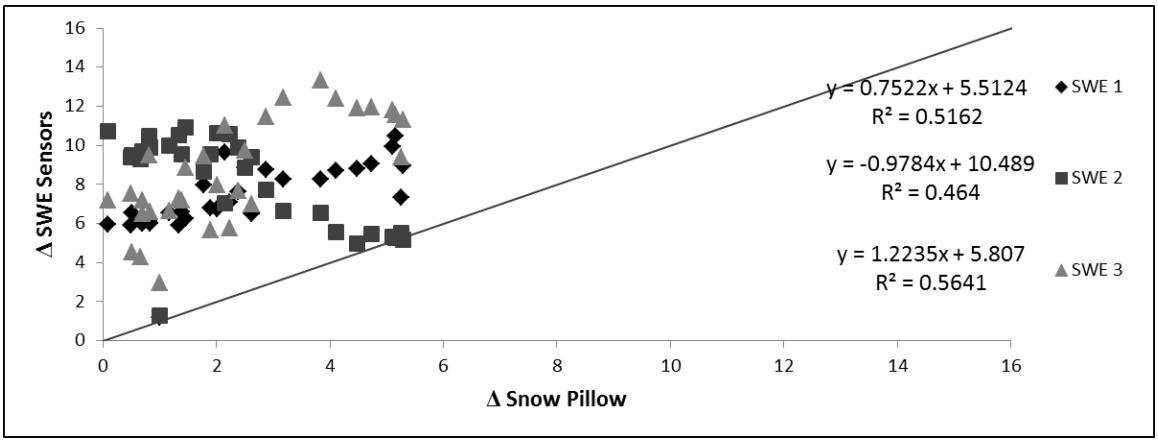

Figure 33. Early-CUES station snow pillow and SWE sensor early season ΔSWE comparison.

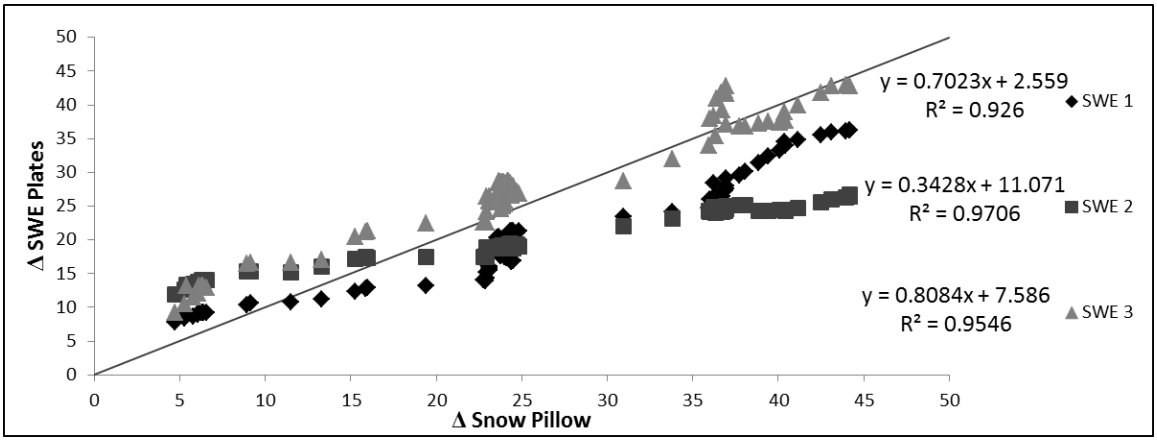

Figure 34. Comparison of the ΔSWE during the accumulation to peak SWE of the three SWE sensors with the snow pillow.

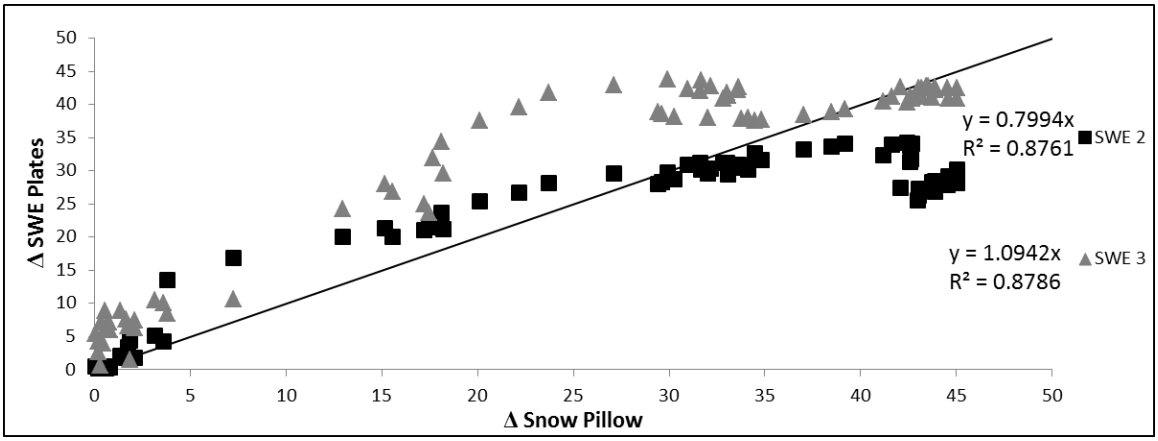

Figure 35. Comparison of ΔSWE of SWE 2 and 3 to the snow pillow during melt phase.

5.3 Sensor Error

The positive response of the SWE sensors during accumulation (i.e., ΔSWE) and clear response to melt has been observed at all sites and all sensors. However, bridging is a common error that occurs with ground based pressure sensors (Johnson 2004b) and was likely evident during several periods during our measurements as discussed above. A very clear example of bridging happened to SWE 1 (Figure 17) in March 2014, which is

examined more closely here (Figure 36). We observe a sharp decline in load cell SWE 1 response and a lack of response to a precipitation event that was captured by the bulk precipitation gage (Figure 36). This error can be attributed to an extended freeze event after the snowpack had been in a melt-freeze cycle as shown by the minimum and maximum temperatures at that time (Figure 36). When the temperature rises sufficiently that bridging ends and there is a return to accurate SWE measurement. Several studies have examined this type of error in both snow pillows as well as load cell ground-based pressure sensors. The underestimation or sudden drops in sensor measurements and subsequent recoveries at Subalpine West in Figures 17 and 36 are consistent with such findings (Johnson 2004a, Johnson et al. 2007, Johnson and Marks 2004). The sun-exposed sensor showed a similar drop and similar recovery after warm temperatures returned (Figure 17 and 37). Another example of sensor error caused by bridging occurred on shaded SWE sensor 3 at the Subalpine West site in April 2015 (Figures 24 and 38).

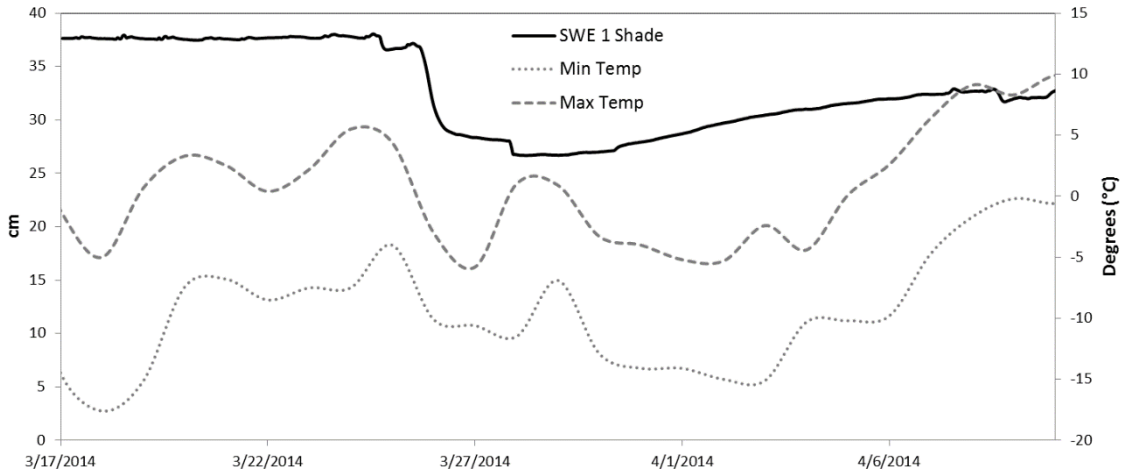

Figure 36. Measurement error due to bridging in March 2014 for SWE 1 at the NevCAN Subalpine West site originally shown in Figure 17.

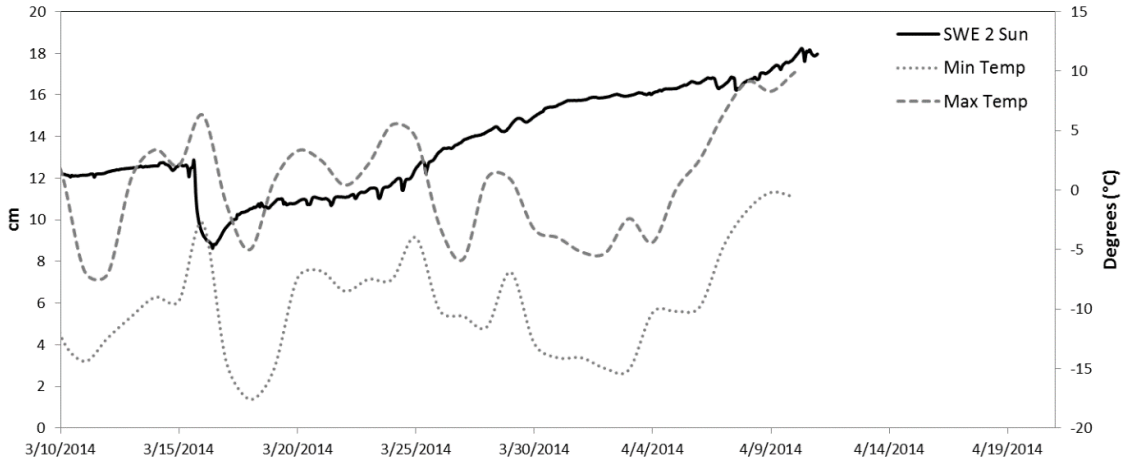

Figure 37. Bridging at the SWE2 sensor at the NevCAN Subalpine West site was caused by physical properties of the snow at the snow/sensor interface.

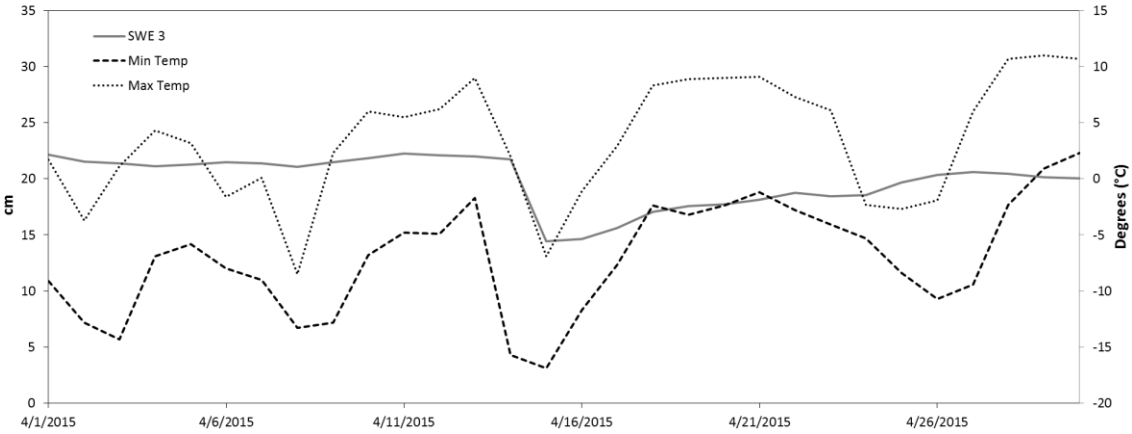

Figure 38. Snow bridging at the Subalpine West site in April 2015 was accompanied by a drop in temperature

Measurement error caused by bridging are the most common errors incurred by ground based pressure sensors and were observed in several sensors during this study, usually accompanied with sudden temperature change (Johnson 2004a, Johnson and Marks 2004, Johnson and Schaefer 2002). All the observed errors caused by snow bridging did resolve over time, on average within two weeks, when temperatures

stabilized and increased. This type of snow bridging is also common with metal bladder snow pillows used by the SNOTEL network, and they have a similar recovery response after the temperature of snowpack increases (verbal conversation with Jeff Anderson, USDA NRCS, Snow Survey and Water Forecasting Program). If necessary, gaps in data can be filled using the equations by Johnson and Marks 2004 using snow depth measurements and a reference density measurement taken when the sensor error occurred (Figure 39). The equation is as follows, with the initial snow density given by,

$$SWE' = \frac{\rho_{ref}}{\rho_w} h_s \qquad (4)$$

where

$$\rho_{ref} = \frac{h_s}{SWE} \rho_w \qquad (5)$$

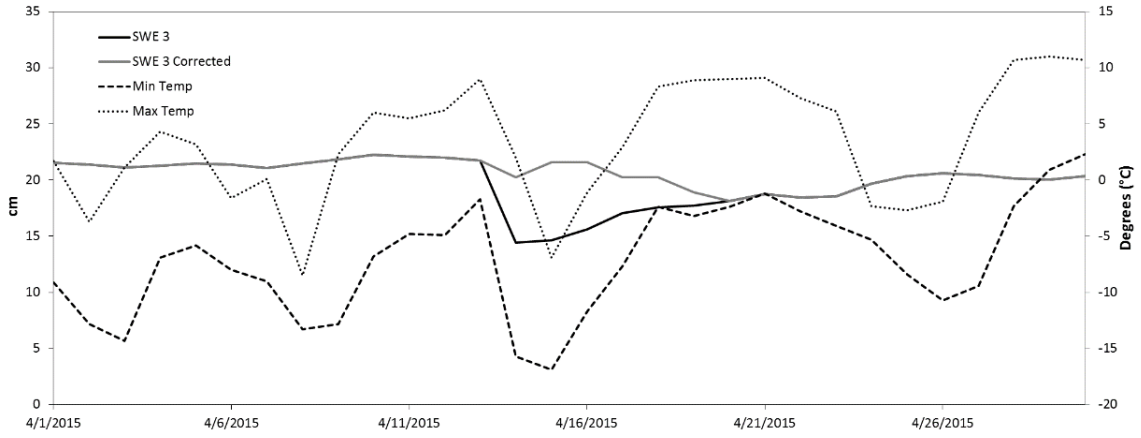

Figure 39. Subalpine West site in April 2015 with data error corrections using the equations of Johnson and Marks 2004.

6. Spatial and Temporal Variability of SWE

6.1 Methods

6.1.1 Spatial Variability Using Manual SWE Measurements

To quantify plot scale spatial variability of SWE, manual snow surveys were performed with a minimum of ten manual SWE measurements during site visits in March 2014, January 2015, February 2015 and March 2015. Initially, core samples were taken directly adjacent to the pressure sensors (March 2014 and January and February 2015). In March 2015, samples were collected in a transect crossing the sensor deployment area in increments of 0.2, 1, 3 and 5 meters. Twenty-seven core samples were collected over a thirty-nine meters at the CUES site in Mammoth CA and sixty core samples were collected over seventy three meters at the NevCAN Subalpine West site. A semi-variogram to calculate the spatial variability of SWE samples was calculated using:

$$\gamma(h) = \frac{1}{2N(h)} \sum_{N(h)} (z_i - z_j)^2 \qquad (6)$$

where h is the lag distance between points; N(h) is the number of distinct pair sets at the lag $h=i-j$; and z_i are measurement values at the locations i. The semi-variogram was used to determine the length at which SWE measurements are auto-correlated (i.e., spatially dependent) and when they become independent. Statistical resampling of independent measurements were conducted to estimate the number of samples needed to obtain a sample within 10% of the SWE population mean. Using MATLAB, a random SWE value was chosen from the complete set of sixty core samples from the Subalpine

West site. Once a sample was chosen, all samples of distance less than the correlation length were discarded and the process restarted. The resampling code was run one thousand times to verify results. Using the federal sampler measurements, both depth and density of the cores were calculated and compared to assess their effective relationship to the SWE measurements. Density was normalized using the equation:

$$\rho_n = \frac{\rho_{snow}}{\rho_{water}} \ . \qquad (7)$$

This equation produces a unitless decimal value that is multiplied by snow height to calculate SWE. All graphic representations in this section show SWE and depth in meters. This decimal form can be compared to the unitless density decimal value.

6.1.2 Spatial and Temporal Variability Using Pressure Sensors

SWE sensor measurements were also used to assess the spatial variability in snowpack. Two sets (<10 m apart) of co-located (<2 m apart) sensors were compared at the NevCAN Subalpine West site. Snow depth time series were created from daily pictures of graduated snow stakes placed next to each SWE sensor. SWE sensors were within ten meters of the snow pillow and placed within three to five meters of each other at the CUES site. Depth measurements were used to determine the normalized density of the snow at each sensor using the equation:

$$\rho_n = \frac{SWE}{h_s}, \qquad (8)$$

where ρ_n is the normalized density of snow and h_s is the height (depth) of snow. The relationship between ρ_n, h_s, and SWE through time was evaluated for each sensor location.

6.2 Results and Discussion: Spatial and Temporal Variability of SWE

6.2.1 Spatial Autocorrelation of SWE

In order to assess spatial patterns of SWE, a semi-variogram was used to define a correlation length for SWE measurements using 60 snow core samples taken on March 21, 2015, at the Sub-alpine West site (Figure 40). A semi-variogram is a function that measures variance and is used to show the correlation of observed measurements. The x-axis is the distance of each sample pair and the y-axis is the calculated variance based on the sum of squares for each set of sample pairs. A lower variance $\gamma(h)$ on the y-axis indicates spatial similarity. Typically, a semi-variogram reaches a sill, at which point measurements are considered spatially unrelated. The jump in distance from the origin is called the nugget and the range is the distance from the sill at which data becomes negligible.

Using the 80 cm correlation length (Figure 40), a Matlab code was written to perform statistical resampling and estimate the number of samples (located at least 80 cm apart to avoid autocorrelation) needed to get within 10% of the transect population mean SWE (0.17 m). Results of statistical resampling show that it takes roughly 10 independent samples to get within 10% of the transect population mean at the Sub-alpine West site (Figure 41). Based on the results of the semi-variogram, all samples taken at <80 cm would be auto-correlated, or similarly, and all samples taken at >80 cm would result in a set of uncorrelated SWE samples. This length becomes important when estimating SWE at the plot scale or over larger watershed areas using ground-based measurements for verification (Meromy et al. 2013b, Molotch and Bales 2005, Watson et al. 2006a).

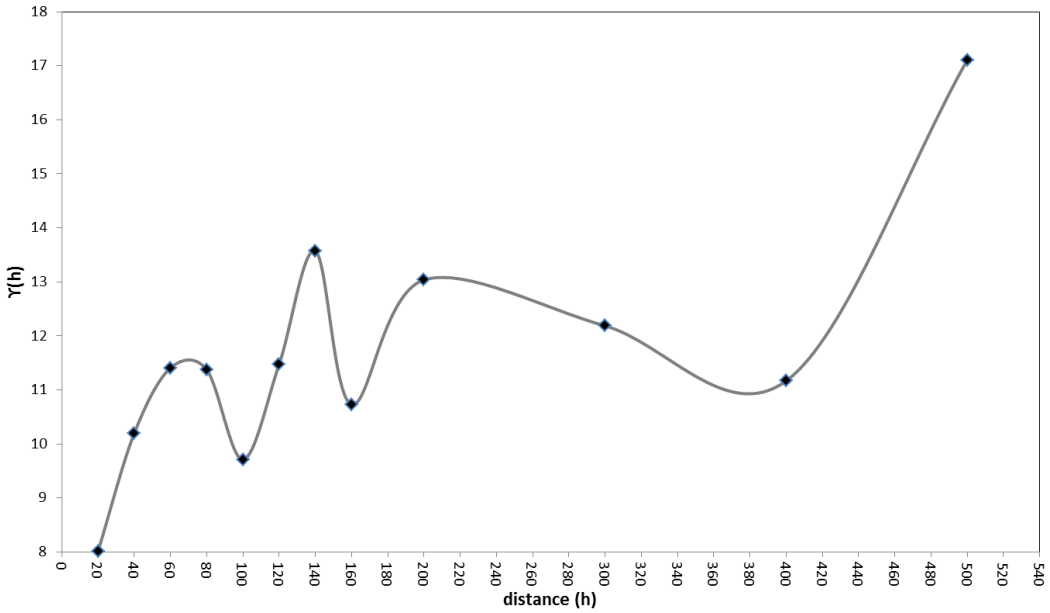

Figure 40. Semi-variogram of SWE using 60 manual core samples taken on March 21, 2015, in the Snake Range, NV.

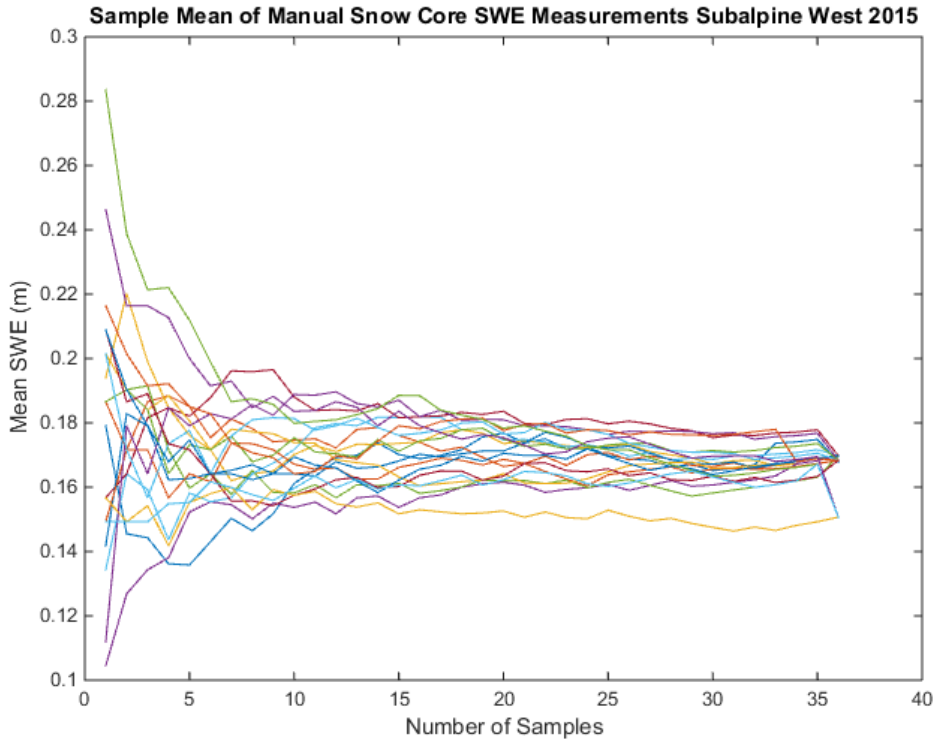

Figure 41. Results of statistical resampling of the 60 snow cores taken at the Sub-alpine West site in March 2015 demonstrate that approximately 10 samples are required to obtain the population mean ≈0.17 m of SWE.

6.2.2 Spatial and Temporal Variability of Depth, Density and SWE

The effect of snow depth and normalized density on the spatial variability of SWE was examined at the Sub-alpine West site (Figures 42 and 43). Manual core samples taken from 20 cm to 5 m apart over the two winter seasons were used to calculate the spatial variability of SWE and its components. The coefficient of variation of SWE from 60 samples taken in March 2015 at Sub-alpine West, a vegetated site in and out of canopy samples, was 22%, with a maximum SWE of 28.3 cm and a minimum of 9.7 cm. Depth and density were examined to estimate their effects on SWE; depth had a coefficient of variability of 19%, ranging from 28 cm to 85 cm, and density had a coefficient of variation of 33%, with normalized density (unitless) between 0.51 and 0.12.

Density has a larger range of relative variability (i.e., relative to its mean value) compared to depth at this site. Figure 42 displays the spatial variability of SWE and its two components, snow depth and normalized density. Depth has greater absolute variability because it has higher values than density; however, density is more variable considering the coefficient of variability.

.

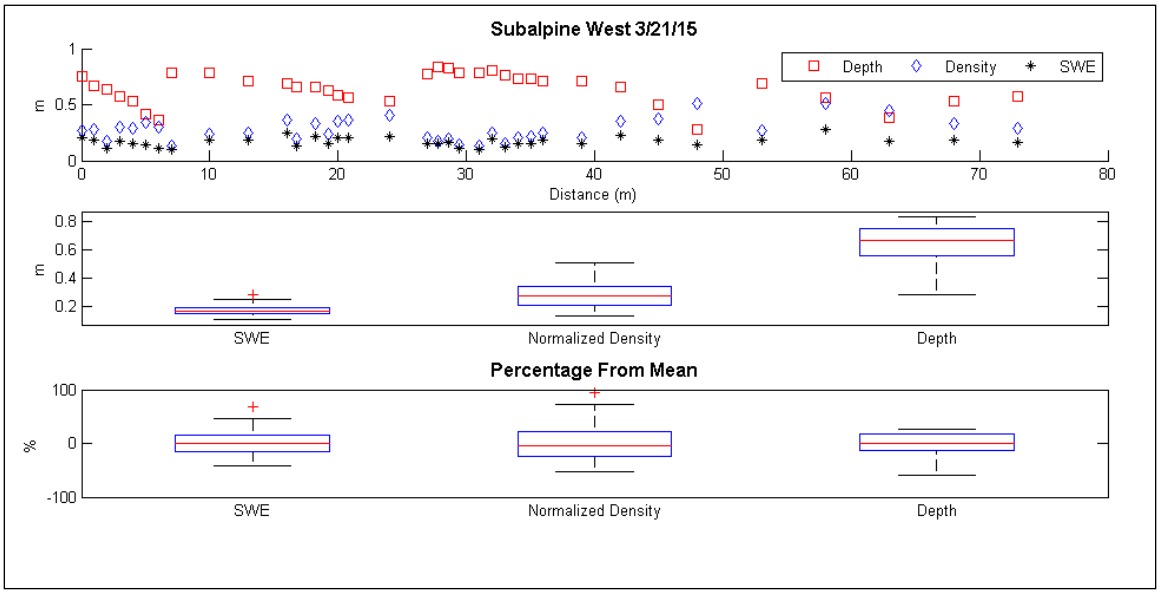

Figure 42. (Top) Depth, density and SWE for 36 independent snow core samples. Boxplots showing the absolute range (middle) and percentage from mean (bottom) in the same variables.

The same calculations were performed at the Mammoth site. This site is an open area with little topographical variation and is considered to be a location where the snowpack would be more homogeneous. The Mammoth site did not have a long enough fetch to acquire sufficient core samples to define a semi-variogram. The 27 samples taken over 39 m in March 2015 (Figure 43) had a coefficient of variation of 25% for SWE, 24% for depth and 15% for density. SWE varied between 8 cm and 38 cm, depth was between 28 cm and 1.30 m, and normalized density was between 0.21 and 0.44.

Unlike Sub-alpine West site, depth was more variable than density at the Mammoth site. As mentioned above, the Mammoth site had less topographical variability than the Sub-alpine West site and the results differ accordingly. Depth is consistent close to the sensor area and decreased as toward the edge of the site. SWE followed the same trend. Overall, the density remained stable in all the samples, only increasing at the shallowest snow depths.

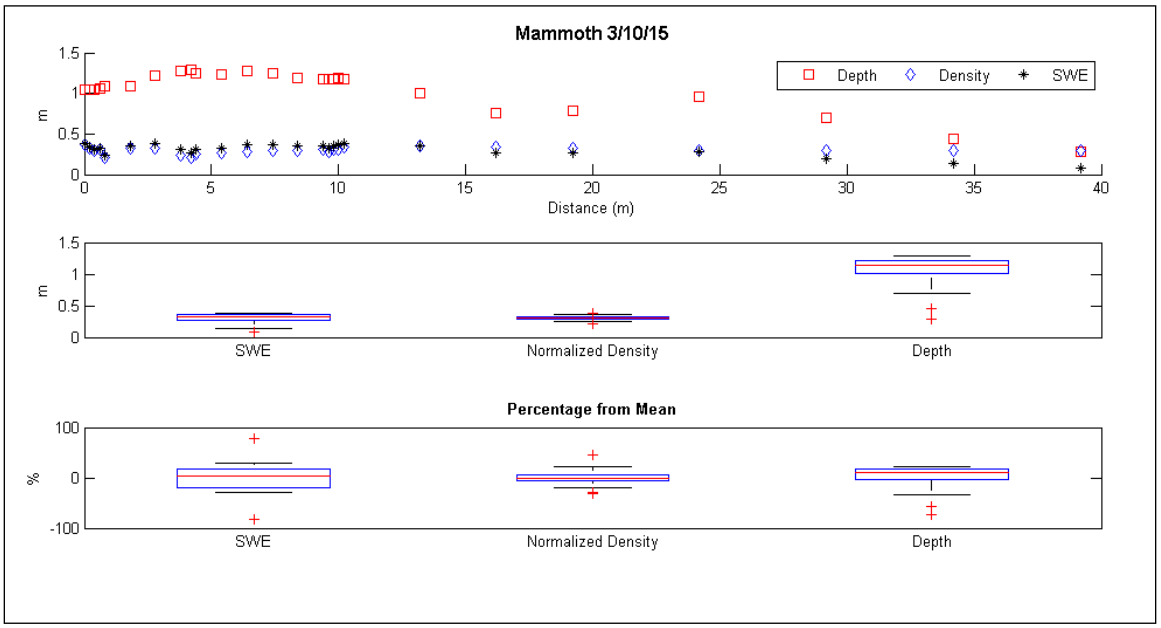

Figure 43. Depth declined at the eastern side of the CUES site transect. The density at this site had less variability, as was expected in the "homogeneous" setting, and SWE was less variable overall as well.

Spatial variability of SWE is not uniform in time, as demonstrated through SWE measurements from both Sub-alpine West and Mammoth in sensors varying from 10 m to <2 m apart (see Figures 24 and 32). Higher variability between sensors developed during the melt-phase process (Figures 44 and 45). Differences in SWE were calculated for the complete time series between the co-located pairs of sensors at the Sub-alpine West site. The shade-protected sensors had smaller seasonal differences until meltoff, when the

northernmost sensor (SWE 1) became snow-free. This created a difference of up to 20 cm of SWE from the sensors. The low r^2 value (0.03) for this set of sensors during melt phase agrees with this assessment, as the high r^2 value of 0.97 from the accumulation to peak shows the steady agreement with small difference in SWE until melt. The differences between the sun-exposed pair of sensors are much more volatile, as melt occurred earlier and more often due to the higher than normal seasonal temperatures and low snowpack. As the sensors experienced larger fluctuation, so did the differences between the sensors. Although this pair had better statistical agreement of melt timing with an r^2 value of 0.75, they showed differences of up to 9 cm of SWE at times during the multiple melt phases. The high variability of snow ablation in forested areas is well known and studied (Davis et al. 1997, Jost et al. 2007), thus giving no reason to think that these differences were due to sensor errors. The pressure sensors show that spatial variability varies with time; the greatest variability occurs during the melt phase. Again this concept supports the need for multiple measurements of SWE during all phases of snowpack evolution in order to make plots of watershed-scale estimates of water equivalent (Kinar and Pomeroy 2015, Sturm et al. 2010, Watson et al. 2006a, Watson et al. 2006b).

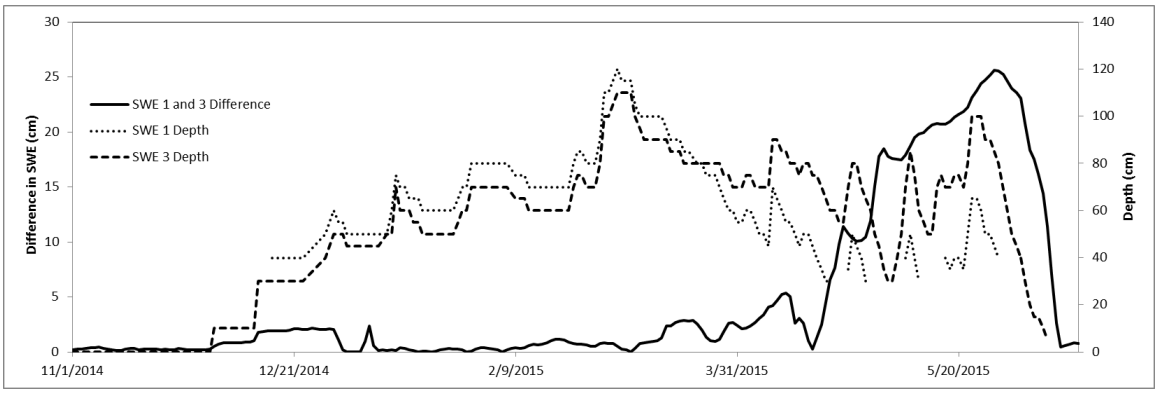

Figure 44. Difference in SWE between sensors located<2m apart.

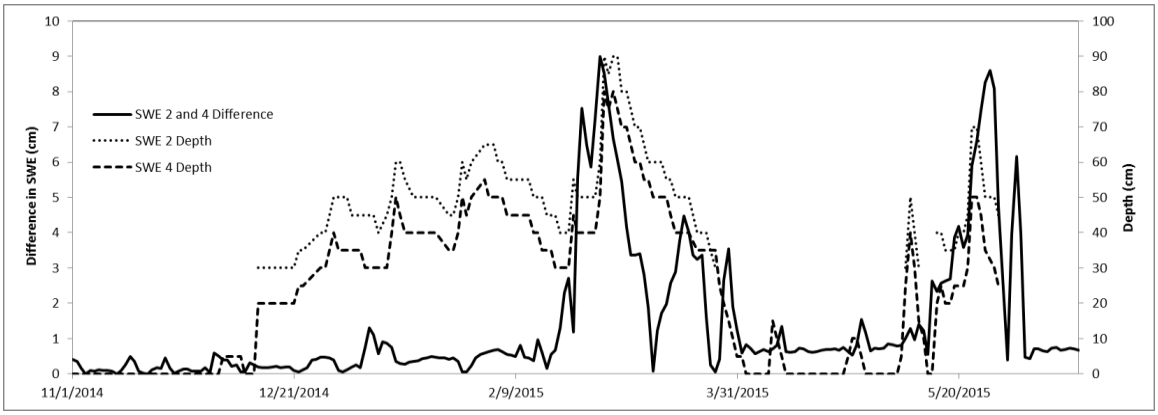

Figure 45. Variability was much higher in the sun-exposed sensor pair due to greater fluctuation in the snowpack.

Manual samples provide depth, density and SWE at one point in time. The pressure sensor data produce a time series that shows the temporal variability of SWE. Using additional depth measurements, snow density can also be calculated. There are fewer density samples taken in snow measurement (Kinar and Pomeroy 2015, López-Moreno et al. 2013, Watson et al. 2006a). Pressure sensor data from Sub-alpine West (Figure 46 and 47) show that depth and density can change considerably over the season, while SWE remains relatively stable. Figure 46 shows the fluctuation of depth and density of the snowpack on the shade-protected sensors. Though SWE remains stable, as

depth decreases density clearly increases. The time series shows that input of new snow lowers density while increasing SWE. Over time the snowpack metamorphoses or "ripens"; this is defined by a change in snow crystal structure. The change in crystal shape is called sintering and the result is an increase in density (DeWalle and Rango 2008). This change is shown very clearly in Figure 46, where in early March, a storm had increased depth by roughly 30 cm. Spring-time sun angle and temperatures initiated ripening and the depth began to drop while density began to increase and SWE stayed relatively stable. The normalized density shown as a percentage of water ($\frac{\rho_{snow}}{\rho_{water}}\ x\ 100$) of the downslope (SWE 3) sensor measurement, which fluctuated over 250% (between 14.48% and 36.66%), and the upslope (SWE 1) sensor, which fluctuated over 380% (between 15.60% and 58.70%). SWE 1 showed the highest density, as it was closer to melt out in the time period shown and thus most likely absorbed the greatest amount of water from the surrounding snowpack (Kinar and Pomeroy 2015). More interesting is the fluctuation in SWE 1 compared to density during the middle of the winter from January 13, 2015, to February 21, 2015. During this time period the SWE increased by 35% (from 12.02 cm to 16.25 cm), whereas the density fluctuated by 80% (from 14.41% to 27.22%), but the key is that it fluctuated through periods of both high and low density in conjunction with the storm and melt cycles. This observation is important when considering variability and lack of snow density measurement and their effects on large-scale SWE estimation (Jonas et al. 2009, Kinar and Pomeroy 2015). As model estimations of SWE are becoming more important and the need for watershed and basin-scale SWE rise in both water balance projections and popularity among water management decision makers, models based on depth measurements do not account for

many of the seasonal changes in density (Jonas et al. 2009, Kinar and Pomeroy 2015, López-Moreno et al. 2013). Furthermore, density in lower-snowpack years does not fluctuate in normal seasonal patterns, with stable measurements in the early, middle and melt phases. Figure 47 shows a graph of the data from the sun-exposed sensor pair SWE 2 and SWE 4, with the depth and density profile. This set of sensors shows an even more pronounced pattern of large fluctuation in density than the shade-protected pair due to continual metamorphosis of the snowpack. Density for SWE 2 fluctuated 400% (between 8.94% and 35.52%) and 350% for SWE 4 (between 12.12% and 42.56%). This clearly shows the plot-scale variability in snowpack as these two sensor pairs are located fewer than 10 m from each other; the change in density is greater in the exposed pair and the SWE is measured at over 6 cm higher in the shade-protected pair. More importantly, these changes in density did not follow the traditional seasonal patterns of early, middle and melt, but instead the density and depth fluctuated over time during both early and middle season and did not increase only with the end-of-season melt phase.

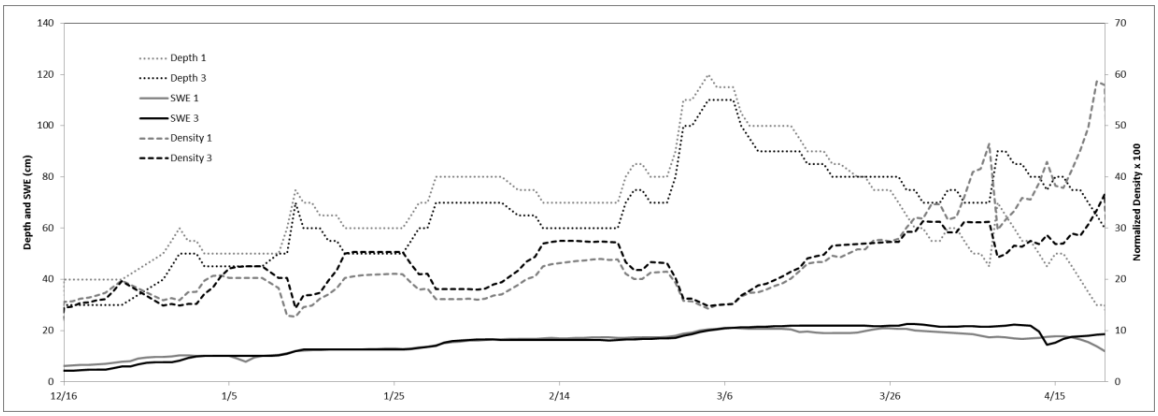

Figure 46. Shade-protected SWE sensor pair at Sub-alpine West, Snake Range, NV. The fluctuation in depth and density over the winter months follows the storm and metamorphosis cycles.

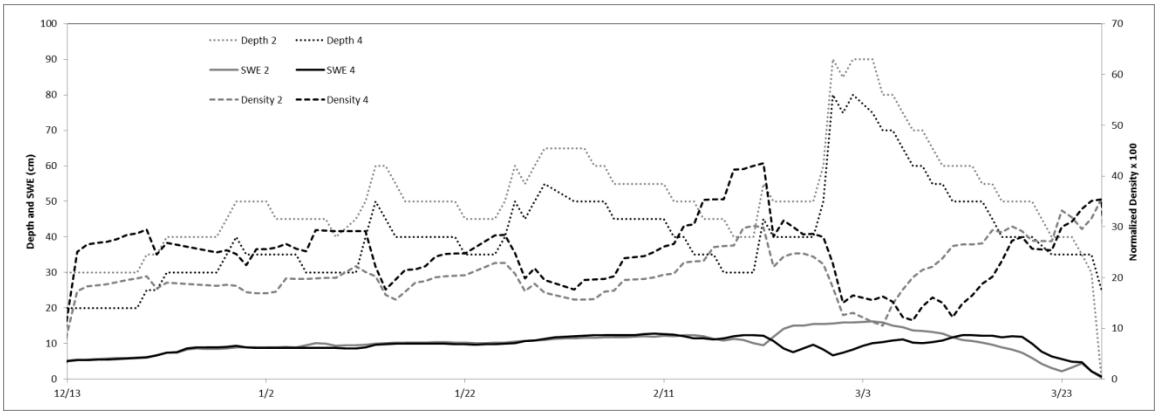

Figure 47. Sun protected pair of SWE sensors with depth and density profiles from Sub-alpine West study site.

7. Conclusions

The new pressure sensor used in this study responded accurately to changes in mass in the laboratory and changes in measured SWE within the variability of manual observations. There was excellent agreement in SWE measurements between paired sensors, specifically during the early season and snowpack accumulation period. The sensors also compared well with snow pillows at two separate sites. Sensors documented high SWE variability during melt phase in forested areas and more spatial homogeneity during the melt cycle in sun exposed areas.

Sensor errors due snow bridging did occur on some sensors during the study. These errors were related to fluctuating temperatures during early melt phase. Erroneous readings in the sensors resolved as temperatures in the snowpack stabilized.

Different levels of sun exposure at the forested study location drove spatial variability of SWE and affected timing of melt. However, “homogeneous” snowpack

also showed spatial SWE variability due to micro-topographical changes. Density had greater variability at the forested site and a greater effect on the change in SWE, whereas depth had more variability at the homogeneous site and a greater effect on SWE change there. Overall, it was observed that mountainous, forested terrain and micro-topography accentuated snowpack variability.

The high variability in SWE measured by both pressure sensors and manual samples suggested that multiple measurements are needed to quantify average SWE. A semi-variogram calculated for one study site using the manual samples suggested an 80 cm SWE correlation length. While snow pillows sample a larger area than the sensors developed for this study, multiple small sensors can be distributed over an entire site.

Finally, snowpack metamorphosis changes the depth and density of the snowpack but this does not always translate into a change in SWE. Use of depth measurements as a proxy for SWE, as has been common practice, can be misleading.

8. References

Association, A.A. (2010) Snow, Weather and Avalanches: Operational Guidelines for Avalanche Programs in the United States, The American Avalanche Association, Pagosa Springs, CO.

Bales, R.C., P., M.N., H., P.T., D., D.M., Robert, R. and Jeff, D. (2006) Mountain hydrology of the western United States. Water Resources Research 42(8), n/a--n/a.

Bormann, K.J., Westra, S., Evans, J.P. and McCabe, M.F. (2013) Spatial and temporal variability in seasonal snow density. Journal of Hydrology 484(0), 63-73.

CDWR (2015) Sierra Nevada Snowpack Is Virtually Gone; Water Content Now is Only 5 Percent of Historic Average, Lowest Since 1950, pp. 1-3, California Department of Water Resources, www.water.ca.gov.

CDWR (1976) Snow Sensor Evaluation in the Sierra Nevada California, Sacramento.

CDWR (2014) Year's Final Snow Survey Comes up Dry; 3-Year Drought Retains Grip as Summer Approaches, pp. 1-3, California Department of Water Resources, www.water.ca.gov.

Clark, M.P., Hendrikx, J., Slater, A.G., Kavetski, D., Anderson, B., Cullen, N.J., Kerr, T., Örn Hreinsson, E. and Woods, R.A. (2011) Representing spatial variability of snow water equivalent in hydrologic and land-surface models: A review. Water Resources Research 47(7), W07539.

Cox, L.M., Bartee, L.D., Crook, A.G., Farnes, P.E. and Smith, J.L. (1978) The Care and Feeding of Snow Pillows, pp. 641-678.

Davis, R.E., Hardy, J.P., Ni, W., Woodcock, C., McKenzie, J.C., Jordan, R. and Li, X. (1997) Variation of snow cover ablation in the boreal forest: A sensitivity study on the effects of conifer canopy. Journal of Geophysical Research: Atmospheres 102(D24), 29389-29395.

DeWalle, D.R. and Rango, A. (2008) Principles of Snow Hydrology, Cambridge University Press, New York.

Dietz, A.J., Kuenzer, C., Gessner, U. and Dech, S. (2012) Remote sensing of snow – a review of available methods. International Journal of Remote Sensing 33(13), 4094-4134.

Dixon, D. and Boon, S. (2012) Comparison of the SnowHydro snow sampler with existing snow tube designs. Hydrological Processes 26(17), 2555-2562.

Doesken, N.J. and Schaefer, G.L. (1987) The Contribution Of SNOTEL Precipitation Measurements To Climate Analysis, Monitoring and Research In Colorado, pp. 20-30, Vancouver BC.

Dozier, J. (2011) Mountain Hydrology, Snow Color, and the Fourth Paradigm. EOS 92(43), 373-384.

Dozier, J. (1989) Spectral signature of alpine snow cover from the landsat thematic mapper. Remote Sensing of Environment 28(0), 9-22.

Elder, K., Dozier, J. and Michaelsen, J. (1991) Snow accumulation and distribution in an Alpine Watershed. Water Resources Research 27(7), 1541-1552.

Grünewald, T. and Lehning, M. (2015) Are flat-field snow depth measurements representative? A comparison of selected index sites with areal snow depth measurements at the small catchment scale. Hydrological Processes 29(7), 1717-1728.

Guan, B., Molotch, N.P., Waliser, D.E., Jepsen, S.M., Painter, T.H. and Dozier, J. (2013) Snow water equivalent in the Sierra Nevada: Blending snow sensor observations with snowmelt model simulations. Water Resources Research 49(8), 5029-5046.

Jepsen, S.M., Molotch, N.P., Williams, M.W., Rittger, K.E. and Sickman, J.O. (2012) Interannual variability of snowmelt in the Sierra Nevada and Rocky Mountains, United States: Examples from two alpine watersheds. Water Resources Research 48, 15.

Jicheng, L., Melloh, R.A., Woodcock, C.E., Davis, R.E., Painter, T.H. and McKenzie, C. (2008) Modeling the View Angle Dependence of Gap Fractions in Forest Canopies: Implications for Mapping Fractional Snow Cover Using Optical Remote Sensing. Journal of Hydrometeorology 9(5), 1005-1019.

Johnson, J.B. (2004a) A theory of pressure sensor performance in snow. Hydrological Processes 18, 53-64.

Johnson, J.B., Gelvin, A. and Schaefer, G.L. (2007) An Engineering Design Study of Electronic Snow Water Equivalent (SWE) Sensor Performance, Kailua-Kona, Hawaii.

Johnson, J.B., Gelvin, A.B., Duvoy, P., Schaefer, G.L., Poole, G. and Horton, G.D. (2014) Performance characteristics of a new electronic snow water equivalent sensor in different climates. Hydrological Processes.

Johnson, J.B. and Marks, D. (2004) The detection and correction of snow water equivalent pressure sensor errors. Hydrological Processes 18(18), 3513--3525.

Johnson, J.B. and Schaefer, G.L. (2002) The influence of thermal, hydrologic, and snow deformation mechanisms on snow water equivalent pressure sensor accuracy. Hydrological Processes 16(18), 3529--3542.

Johnson, J.B.a.M.D. (2004b) The detection and correction of snow water equivalent pressure sensor errors. Hydrological Processes 18(18), 3513--3525.

Johnson, J.B.a.S.G.L. (2002) The influence of thermal, hydrologic, and snow deformation mechanisms on snow water equivalent pressure sensor accuracy. Hydrological Processes 16(18), 3529--3542.

Jonas, T., Marty, C. and Magnusson, J. (2009) Estimating the snow water equivalent from snow depth measurements in the Swiss Alps. Journal of Hydrology 378(1–2), 161-167.

Jost, G., Moore, R.D., Weiler, M., Gluns, D.R. and Aluila, Y. (2009) Use of Distributed Snow Measurements to Test and Improve a Snowmelt Model for Predicting the Effect of Forest Clear-cutting. Journal of Hydrology (376), 94-106.

Jost, G., Weiler, M., Gluns, D.R. and Alila, Y. (2007) The influence of forest and topography on snow accumulation and melt at the watershed-scale. Journal of Hydrology 347(1–2), 101-115.

Kinar, N.J. and Pomeroy, J.W. (2015) MEASUREMENT OF THE PHYSICAL PROPERTIES OF THE SNOWPACK. Reviews of Geophysics, n/a-n/a.

Klos, P.Z., Link, T.E. and Abatzoglou, J.T. (2014) Extent of the rain-snow transition zone in the western U.S. under historic and projected climate. Geophysical Research Letters 41(13), 4560-4568.

Kumar, M., Marks, D., Dozier, J., Reba, M. and Winstral, A. (2013) Evaluation of distributed hydrologic impacts of temperature-index and energy-based snow models. Advances in Water Resources 56, 77-89.

Liston, G.E. (2004) Representing Subgrid Snow Cover Heterogeneities in Regional and Global Models. Journal of Climate 17(6), 1381-1397.

López-Moreno, J.I., Fassnacht, S.R., Heath, J.T., Musselman, K.N., Revuelto, J., Latron, J., Morán-Tejeda, E. and Jonas, T. (2013) Small scale spatial variability of snow density and depth over complex alpine terrain: Implications for estimating snow water equivalent. Advances in Water Resources 55(0), 40-52.

Marks, D., Adam, W. and Mark, S. (2002) Simulation of terrain and forest shelter effects on patterns of snow deposition, snowmelt and runoff over a semi-arid mountain catchment. Hydrological Processes 16(18), 3605--3626.

Meromy, L., Molotch, N.P., Link, T.E., Fassnacht, S.R. and Rice, R. (2013a) Subgrid variability of snow water equivalent at operational snow stations in the western USA. Hydrologic Processes 27, 2383-2400.

Meromy, L., Molotch, N.P., Link, T.E., Fassnacht, S.R. and Rice, R. (2013b) Subgrid variability of snow water equivalent at operational snow stations in the western USA. Hydrological Processes 27(17), 2383-2400.

Molotch, N.P. and Bales, R.C. (2005) Scaling snow observations from the point to the grid element: Implications for observation network design. Water Resources Research 41.

Molotch, N.P., Brooks, P.D., Burns, S.P., Litvak, M., Monson, R.K., McConnell, J.R. and Musselman, K. (2009) Ecohydrological controls on snowmelt partitioning in mixed-conifer sub-alpine forests. Ecohydrology 2(2), 129-142.

Mote, P.W., Hamlet, A.F., Clark, M.P. and Lettenmaier, D.P. (2005) DECLINING MOUNTAIN SNOWPACK IN WESTERN NORTH AMERICA*. Bulletin of the American Meteorological Society 86(1), 39-49.

NASA (2014) NASA Airborne Snow Observatory, NASA Jet Propulsion Laboratory.

Nevada, U.i. (2012) A Guide to the Papers of James Edward Church Collection No.NC96. Searcy, S. (ed), University of Nevada Reno.

Pomeroy, J.W., Gray, D.M. (1995) Snowcover Accumulation, Relocation and Management, National Hydrology Research Institute, Saskatoon, Saskatchewan, Canada.

Rasmus, S. (2013) Spatial and Temporal Variability of Snow Bulk Density and Seasonal Snow Densification Behavior in Finland. Geophysica 49(1-2), 53-74.

Rice, R. and Bales, R.C. (2010) Embedded-sensor network design for snow cover measurements around snow pillow and snow course sites in the Sierra Nevada of California. Water Resources Research 46.

Rice, R., C., B.R., H., P.T. and Jeff, D. (2011) Snow water equivalent along elevation gradients in the Merced and Tuolumne River basins of the Sierra Nevada. Water Resources Research 47(8), n/a--n/a.

Savina, M., Schäppi, B., Molnar, P., Burlando, P. and Sevruk, B. (2012) Comparison of a tipping-bucket and electronic weighing precipitation gage for snowfall. Atmospheric Research 103, 45-51.

Sturm, M. and Holmgren, J. (1998) Differences in compaction behavior of three climate classes of snow. Annals of Glaciology 26, 126-130.

Sturm, M., Holmgren, J. and Liston, G.E. (1995) A Seasonal Snow Cover Classification System for Local to Global Applications. Journal of Climate 8(5), 1261-1283.

Sturm, M., Taras, B., Liston, G.E., Derksen, C., Jonas, T. and Lea, J. (2010) Estimating Snow Water Equivalent Using Snow Depth Data and Climate Classes. Journal of Hydrometeorology 11(6), 1380-1394.

Viviroli, D., Archer, D.R., Buytaert, W., Fowler, H.J., Greenwood, G.B., Hamlet, A.F., Huang, Y., Koboltschnig, G., Litaor, M.I., López-Moreno, J.I., Lorentz, S., Schädler, B., Schreier, H., Schwaiger, K., Vuille, M. and Woods, R. (2011) Climate change and mountain water resources: overview and recommendations for research, management and policy. Hydrology & Earth System Sciences 15(2), 471-504.

Watson, F.G.R., Anderson, T.N., Newman, W.B., Alexander, S.E. and Garrott, R.A. (2006a) Optimal sampling schemes for estimating mean snow water equivalents in stratified heterogeneous landscapes. Journal of Hydrology 328(3–4), 432-452.

Watson, F.G.R., Newman, W.B., Coughlan, J.C. and Garrott, R.A. (2006b) Testing a distributed snowpack simulation model against spatial observations. Journal of Hydrology 328(3–4), 453-466.

Winkler, R.D., Spittlehouse, D.L. and Golding, D.L. (2005) Measured differences in snow accumulation and melt among clearcut, juvenile, and mature forests in southern British Columbia. Hydrological Processes 19(1), 51-62.

Yang, D., Kane, D.L., Hinzman, L.D., Goodison, B.E., Metcalfe, J.R., Louie, P.Y.T., Leavesley, G.H., Emerson, D.G. and Hanson, C.L. (2000) An evaluation of the Wyoming Gauge System for snowfall measurement. Water Resources Research 36(9), 2665-2677.

Zito, K. (2011) Sierra snowpack is one of the biggest on record, San Francisco, CA.